NEUROSCIENCE

Intracellular delivery of Parkin rescues neurons from accumulation of damaged mitochondria and pathological α-synuclein

Eunna Chung[1]*, Youngsil Choi[1]*, Jiae Park[1], Wonheum Nah[1], Jaehyung Park[1], Yukdong Jung[1], Joonno Lee[1], Hyunji Lee[1], Soyoung Park[1], Sunyoung Hwang[1], Seongcheol Kim[1], Jongseok Lee[1], Dongjae Min[1], Junghwan Jo[1], Shinyoung Kang[1], Minyong Jung[1], Phil Hyu Lee[2], H. Earl Ruley[3], Daewoong Jo[1†]

Parkinson's disease (PD) is a progressive neurodegenerative disorder characterized by mitochondrial dysfunction, Lewy body formation, and loss of dopaminergic neurons. Parkin, an E3 ubiquitin ligase, is thought to inhibit PD progression by removing damaged mitochondria and suppressing the accumulation of α-synuclein and other protein aggregates. The present study describes a protein-based therapy for PD enabled by the development of a cell-permeable Parkin protein (iCP-Parkin) with enhanced solubility and optimized intracellular delivery. iCP-Parkin recovered damaged mitochondria by promoting mitophagy and mitochondrial biogenesis and suppressed toxic accumulations of α-synuclein in cells and animals. Last, iCP-Parkin prevented and reversed declines in tyrosine hydroxylase and dopamine expression concomitant with improved motor function induced by mitochondrial poisons or enforced α-synuclein expression. These results point to common, therapeutically tractable features in PD pathophysiology, and suggest that motor deficits in PD may be reversed, thus providing opportunities for therapeutic intervention after the onset of motor symptoms.

INTRODUCTION

Parkinson's disease (PD) and Parkinson-like diseases belong to a family of neurodegenerative disorders characterized by the loss of dopaminergic neurons, leading to clinical symptoms such as exercise relaxation, tremor, and postural instability (*1*). The diseases present in a variety of ways, which has confounded efforts to understand the underlying pathophysiology. Sporadic PD has been linked to the spread of α-synuclein–containing Lewy bodies (and associated neurodegeneration) that spread from the olfactory bulb and the medulla oblongata in the central nervous system (*2*) to the pontine tegmentum, the midbrain, and the amygdala, at which point, the pathognomonic motor symptoms of PD appear. Aggregated or overexpressed α-synuclein induces similar pathology in experimental animals (*3*). Familial early-onset PD is linked to genetic mutations in proteins such as Parkin and phosphatase and tensin homolog (PTEN)–induced kinase 1 (PINK1) that regulate mitophagy, a process to remove damaged mitochondria, which protect against PD (*4*, *5*). However, Lewy bodies are not observed in familial PD or in knockout (KO) mice bearing analogous mutations. Likewise, Lewy bodies are not observed in parkinsonian conditions induced in animals and humans by mitochondrial poisons such as 1-methyl-4-phenyl-1,2,3,6-tetrahydropyridine (MPTP) and rotenone. These differences have raised questions about the relevance of different animal models to sporadic PD and the development of mechanism-based therapies to treat the disease. Moreover, there is widespread concern that by the time motor symptoms appear, which is when the disease is normally diagnosed, the pathology has become irreversible (*6*).

Parkin functions as an E3 ubiquitin ligase and acts downstream of PINK1 and protein deglycase (DJ-1) in the damage-induced mitophagy response (*4*, *5*, *7*). Enforced Parkin gene expression has been shown to suppress PD phenotypes in a variety of cell and animal models following acute intoxication with mitochondrial poisons or exposure to aggregated α-synuclein (*8*–*10*). These findings suggest that Parkin could provide an effective PD therapy, assuming (i) practical methods can be developed to deliver Parkin to affected areas of the brain, and (ii) the damage to dopaminergic neurons can be arrested (or reversed) by this treatment after the onset of motor symptoms (*3*, *5*, *7*, *11*).

The present study addressed both of these goals. First, we describe the development of an efficient therapeuticmolecule systemic delivery technology (TSDT) to deliver proteins into mammalian cells and tissues. Specifically, sequence-optimized advanced macromolecule transduction domains (aMTDs) were developed to facilitate efficient bidirectional transport of proteins across the plasma membrane and allow systemic protein delivery to a variety of tissues, including the brain. Second, we developed an improved cell-permeable Parkin (iCP-Parkin) by attaching an aMTD sequence and a solubilization domain (SD) to the full-length human Parkin protein. Purified recombinant iCP-Parkin protein displayed a high level of cell permeability that was aMTD dependent and maintained the E3 ubiquitin ligase activity of native Parkin. Most importantly, iCP-Parkin (but not control proteins without the aMTD sequence) suppressed neuronal toxicity in cultured cells and animals exposed to mitochondrial poisons and aggregated α-synuclein. The response included a restoration of tyrosine hydroxylase (TH)–positive dopaminergic neuronal cells in the striatum and the midbrain, concomitant with enhanced dopamine (DA) expression and restoration of gross motor function. These results suggest common therapeutically tractable features in the pathophysiology of PD and Parkinson-like diseases and show that the motor deficits in PD may not be as irreversible as often assumed.

[1]Cellivery R&D Institute, Cellivery Therapeutics Inc., Seoul 03929, Korea. [2]Department of Neurology, Yonsei University College of Medicine, Seoul 120-752, Korea. [3]Department of Pathology, Microbiology & Immunology, Vanderbilt University School of Medicine, Nashville, TN 37232, USA.
*These authors contributed equally to this work
†Corresponding author. Email: ceo@cellivery.com

RESULTS

Enhanced protein delivery with sequence-optimized aMTDs

While a variety of hydrophobic sequences have been empirically found to enhance the delivery of protein cargos into cells and tissues (*12*, *13*), we identified six critical factors: amino acid length, bending potential (proline presence and location), rigidity/flexibility (instability index), aliphatic index, hydropathy [grand average of hydropathy (GRAVY)], and the location of hydrophobic and aliphatic residues that contributed to optimal protein delivery (table S1). After excluding sequences with outlying values for bending potential, rigidity, and hydrophobicity, we determined the average values and ranges for each of the six critical factors and synthesized 136 synthetic peptides (designated aMTDs) that covered a range of values for each critical factor (table S1). These included otherwise consensus-conforming peptides from which at least one of the critical factors was omitted [unsatisfying peptides (uPs)]. Each peptide was tested for its ability to deliver a fluorescein isothiocyanate (FITC)–labeled reporter protein into RAW264.7 cells. Protein uptake was measured by flow cytometry and confocal laser scanning microscopy. The uPs engineered beyond certain conditions of denoted critical factors or with varied bending potentials depending on proline were largely unable to enhance protein delivery (fig. S1, A and C). As illustrated in fig. S1B, aMTDs that satisfied all critical factors (aMTD910) demonstrated up to 13-fold greater cell permeability than previous hydrophobic transduction peptides such as membrane translocating motif (MTM) and macromolecule transduction domain 85 (MTD85).

Development of a cell-permeable Parkin with enhanced solubility

An earlier study described a cell-permeable Parkin able to protect mice from chemically induced PD. However, the protein suffered from low solubility and was therefore unsuited for clinical development. To develop a cell-permeable Parkin with enhanced therapeutic potential, the protein was modified in three steps. First, we added a 99–amino acid protein solubilization domain B (SDB), derived from cytochrome b of *Rattus norvegicus*. This domain had been previously shown to enhance the solubility of recombinant proteins (*14*). Second, aMTD524-Parkin-SDB (Fig. 1A) was selected for the current study with the desired combination of solubility and cell delivery. Together, these steps illustrate practical application of the TSDT platform.

Mechanism of aMTD-mediated protein delivery

As assessed by flow cytometry and fluorescence/confocal microscopy, iCP-Parkin was highly cell permeable in a dose- and time-dependent manner, whereas the same protein without an aMTD or dye only was not, suggesting that the aMTD sequence is essential for intracellular and systemic delivery (Fig. 1, B and C, and fig. S2, A to C and E). aMTD-dependent iCP-Parkin delivery was observed in all cell types examined including primary mouse neurons (Fig. 1C) as well as human neuronal (SH-SY5Y) and astrocyte (NHA) cells (Fig. 1B and fig. S2C). Uptake was decreased by EDTA treatment (Fig. 1D) and low temperature (Fig. 1E) but was unaffected by depleting cells of adenosine 5′-triphosphate (ATP; Fig. 1F) or surface proteins (Fig. 1G), or by inhibitors of microtubule cytoskeleton (Fig. 1H), clathrin-dependent endocytosis (Fig. 1I), macropinocytosis (Fig. 1J), or lipid raft–dependent uptake (Fig. 1K). In short, aMTD-mediated protein delivery appeared to involve direct penetration of an intact lipid bilayer by an energy-independent mechanism.

We reasoned that if aMTD-containing cargos penetrate the plasma membrane directly, then the proteins should be capable of bidirectional movement in and out of cells. To test this possibility, C2C12 cells were pretreated with FITC-labeled iCP-Parkin washed to remove noninternalized protein and mixed with RAW264.7 cells bound to a phycoerythrin (PE)–labeled anti-CD14 antibody. The appearance of flow-sorted double-positive FITC/PE suggests that iCP-Parkin exited C2C12 cells and entered neighboring RAW264.7 cells (Fig. 1L). Next, we questioned whether cell-to-cell transfer involved biologically active protein, which proved to be the case as cells preloaded with iCP-Parkin exerted a protective effect on neighboring neurotoxin-treated cells (Fig. 1M).

iCP-Parkin is intracellularly delivered to deep brain tissues

To examine systemic protein delivery, iCP-Parkin and non–CP-Parkin (a control Parkin protein without the aMTD sequence) were labeled with FITC, administered intravenously, and the fluorescent signal was monitored in major organs including the brain, liver, heart, kidney, lung, and spleen. Florescent signal was observed in all tissues examined but only in mice injected with FITC-labeled iCP-Parkin (fig. S2E). We next evaluated the distribution of Cy5-labeled iCP-Parkin after intravenous injection to nude mice using an in vivo imaging system (IVIS). In fig. S2D, strong fluorescence of Cy5-labeled iCP-Parkin was detected in the entire body including the brain region at 3 hours after injection compared with mice that received Cy5 only. The fluorescence intensity gradually weakened over time. In fig. S2D, excised brains from Cy5-labeled iCP-Parkin–treated mice showed stronger Cy5 fluorescence signals than controls.

iCP-Parkin was detected in both the substantia nigra and striatum as assessed by Western blot (Fig. 2A; analyzed also in the whole-brain sample) and enzyme-linked immunosorbent assay (ELISA) analysis (Fig. 2B). Maximum levels of iCP-Parkin (56.4 ng/g is present at 2 hours in striatum) were observed 2 hours after injection (Fig. 2, A and B), and the protein was colocalized with markers for neurons (Fig. 2C), astrocytes (fig. S2F), and microglia (fig. S2G), including TH-positive (dopaminergic) neurons of the substantia nigra (fig. S2H).

The kinetics of iCP-Parkin delivery to the brain was also assessed by using liquid chromatography–tandem mass spectrometry (LC-MS/MS) to detect a unique peptide (AVALIVVPALAPMIVFVR) from the iCP-Parkin N terminus (Fig. 2, D and E). The maximum amount of iCP-Parkin was detected at the 30-min time point in the whole-brain samples of the normal mouse model (Fig. 2E) and showed gradually decreased levels over time (up to 24 hours). Together, these data suggest that iCP-Parkin crosses the blood-brain barrier (BBB) and is intracellularly delivered to deep brain tissues.

iCP-Parkin autoubiquitination and cytoprotective activities do not require PINK1

Since PINK1 activates Parkin by phosphorylation-induced conformational changes, we considered the possibility that iCP-Parkin might be in a constitutively active conformation, for example, due to refolding during purification or removal of N-terminal sequences (*15*). Although iCP-Parkin could serve as a substrate for PINK1 as determined by Western blot analysis probing with an anti–pSer^{65}-Parkin antibody (fig. S3A), the unphosphorylated protein was active as an E3 ubiquitin ligase (fig. S3B). Ser^{65} phosphorylation was enhanced in cells overexpressing PINK1 and further increased by treatment with carbonyl cyanide *m*-chlorophenyl hydrazone (CCCP),

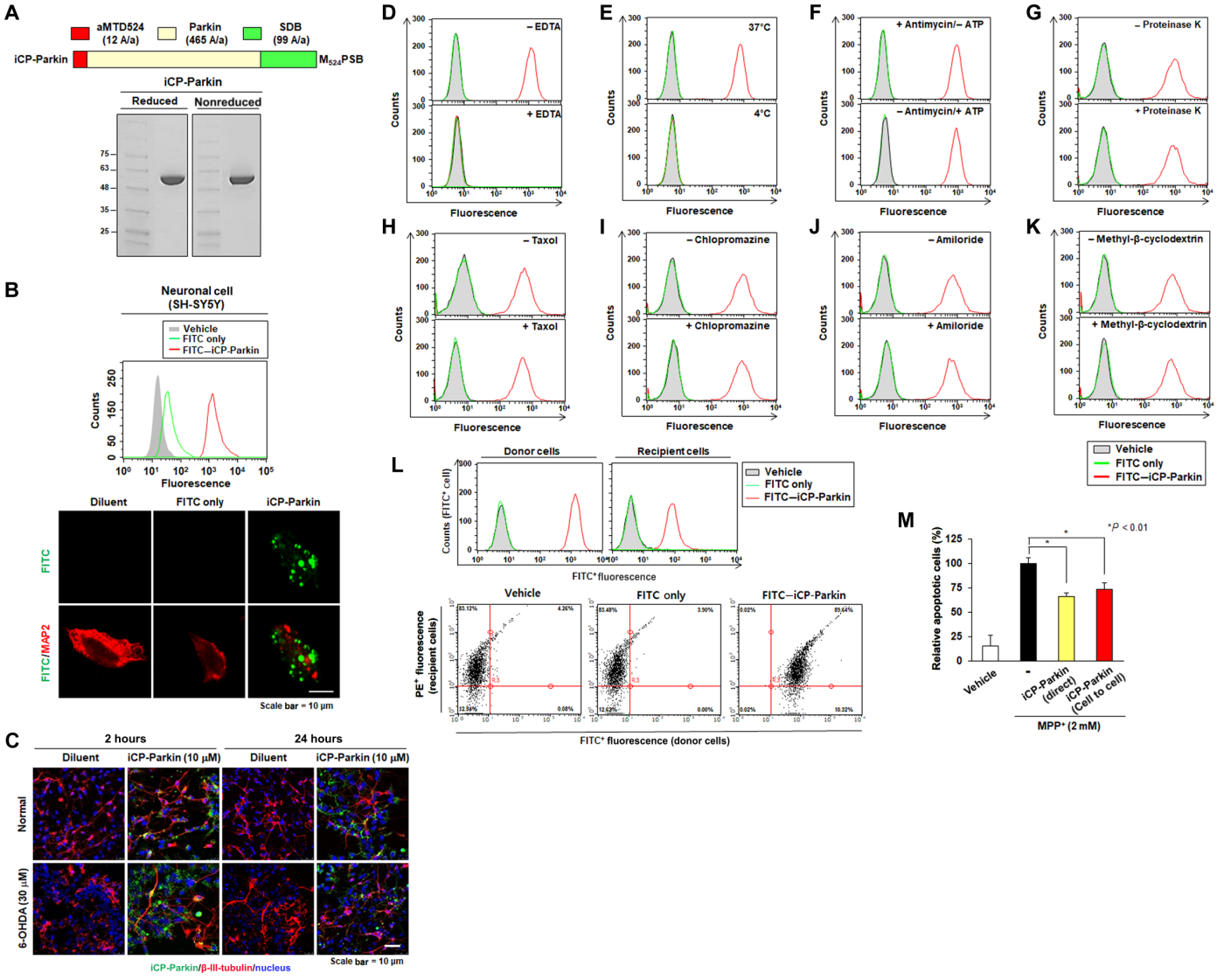

Fig. 1. Purification and characterization of iCP-Parkin; aMTD/SD-fused Parkin recombinant protein is cell permeable via direct cell-to-cell transfer. (**A**) Structure of Parkin recombinant proteins fused to aMTD524 and SDB (iCP-Parkin). SDS-PAGE (reducing and nonreducing) image of iCP-Parkin. (**B**) Neuronal (SH-SY5Y cell) measured by flow cytometry and confocal laser scanning microscopy, demonstrating the intracellular localization of iCP-Parkin. (**C**) Immunofluorescence staining data (green fluorescence) showing intracellular location of iCP-Parkin in primary neurons when cotreated with or without 6-OHDA at 2 and 24 hours. β-III-Tubulin was also costained and detected as red fluorescent signal. The representative data are presented, and the tests were carried out in quadruplicate ($n = 4$). aMTD-mediated delivery of iCP-Parkin is notably affected by EDTA treatment (**D**) and low temperature (**E**) but unaffected by pretreatment of cells with the ATP-depleting agent antimycin (**F**), proteinase K (**G**), the microtubule inhibitor Taxol (**H**), a clathrin-mediated endocytosis blocker, chlorpromazine (**I**), a macropinocytosis blocker, amiloride (**J**), or a lipid raft–mediated endocytosis blocker, methyl-β-cyclodextrin (**K**). (**L**) Cell-to-cell transfer of iCP-Parkin. C2C12 cells (donor cells) were pretreated with FITC–iCP-Parkin (green) for 2 hours and were mixed with RAW264.7 cells (recipient cells) labeled with PE-CD14 antibody (red) for 2 hours. Green/red fluorescent double-positive cells were analyzed by flow cytometry. (**M**) The cytoprotective effect of iCP-Parkin via cell-to-cell transfer. iCP-Parkin–treated SH-SY5Y cells (for 2 hours) incubated with GFP-transfected SH-SY5Y cells for 6 hours. These mixed cells were treated with 2 mM MPP^+ for 24 hours. Apoptosis of GFP-positive cells was analyzed by an annexin V/7-AAD apoptosis detection assay. Quantification of cytoprotective effect by cell-to-cell transferred iCP-Parkin. Data are represented as the means ± SD with Student's *t* test.

a mitochondrial uncoupling agent (fig. S3C). Low levels of basal and CCCP-induced $pSer^{65}$ reactivity observed in PINK1 KO cells (fig. S3D) presumably involve kinases other than PINK1. Last, PINK1 wild-type (WT) and KO cells were similarly sensitive to CCCP treatment and to iCP-Parkin cytoprotection (fig. S3E), further suggesting that iCP-Parkin function is uncoupled from PINK1 regulation.

iCP-Parkin induces mitophagy and mitochondrial biogenesis

In principle, therapeutic proteins provide a way to regulate biochemical functions in cells and tissues under non–steady-state conditions and directly influence biochemical pathways responsible for disease pathophysiology. A series of experiments were performed to determine the extent to which iCP-Parkin functions like native Parkin (Fig. 3A), which acts downstream of PINK1 and DJ-1 in the damage-induced

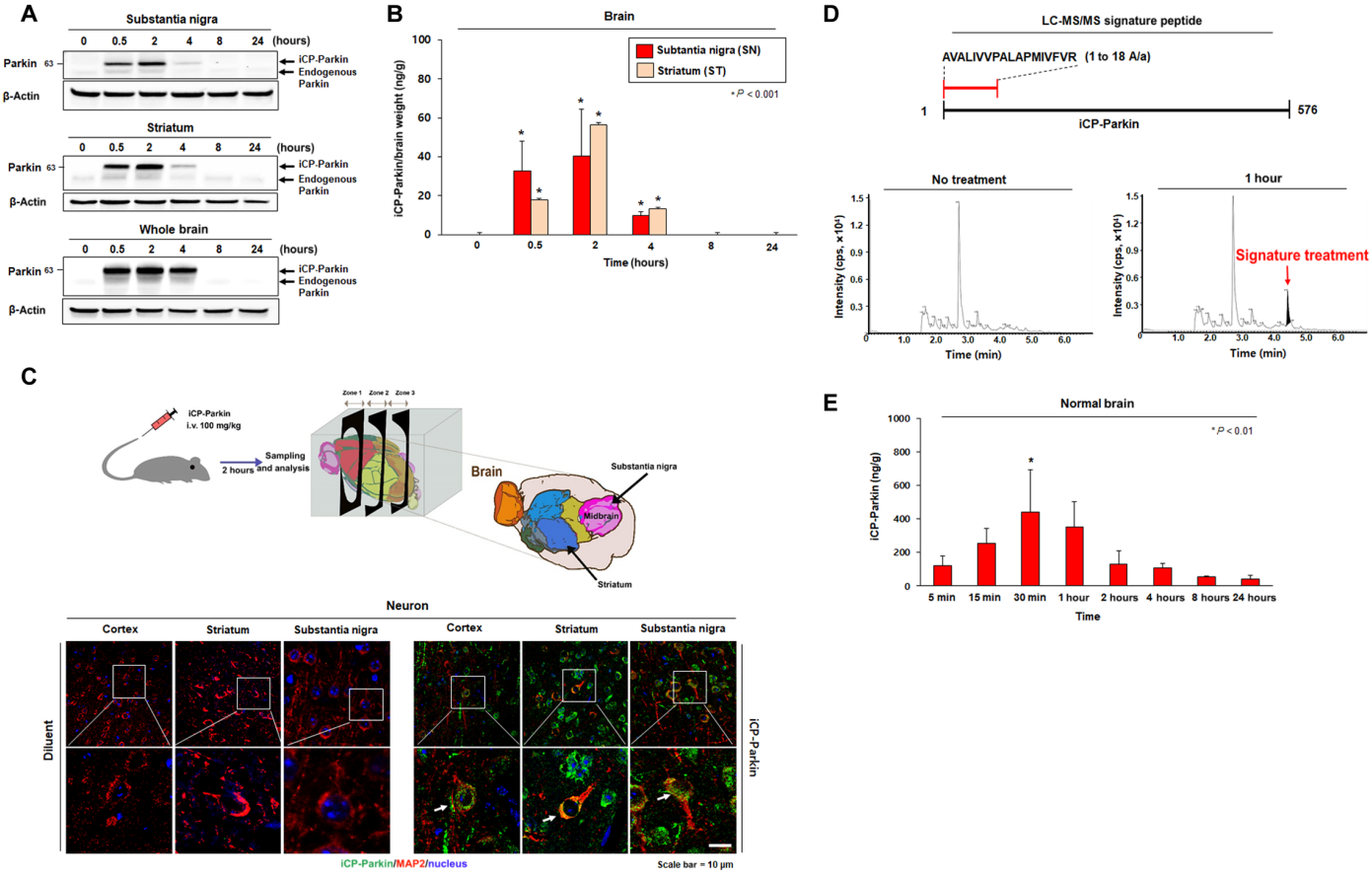

Fig. 2. iCP-Parkin is delivered to the brain through the BBB. (**A** and **B**) Time course analysis of brain tissue permeability. The level of each protein in the brain tissue was measured by Western blot (A) and ELISA (B) ($n = 3$). All analysis samples were collected after intravenous injection of iCP-Parkin (100 mg/kg). The molecular weights of iCP-Parkin and endogenous Parkin are 63 and 53 kDa, respectively. Western blot analysis of substantia nigra and striatum tissues was carried out in triplicate. *$P < 0.001$ versus 0 hour (B). (**C**) Immunohistochemistry for iCP-Parkin in mouse cortex, striatum, and substantia nigra after intravenous (i.v.) injection of iCP-Parkin. Anti-Parkin antibody and anti-MAP2 antibody for neurons. Scale bar, 10 μm. (**D**) LC-MS/MS analysis detecting iCP-Parkin in the mouse brain. The mass spectrometry peak (filled with black color) shows an iCP-Parkin peptide (AVALIVVPALAPMIVFVR) containing aMTD 524. Time point: 0 and 30 min. (**E**) Quantified amounts of iCP-Parkin detected in brain samples of normal mouse by LC-MS/MS at varied time points ($n = 5$). Time point: 5, 15, and 30 min, and 1, 2, 4, 8, and 24 hours. *$P < 0.01$ versus 24 hours. Data in (B) and (E) are the means ± SD with Student's *t* test, respectively.

mitophagy pathway (*4*, *5*, *7*) and plays a broadly protective role in maintaining neuronal cell function and viability (*16*–*19*).

First, iCP-Parkin physically interacted with endogenous PINK1 in response to toxin treatment (Fig. 3B) and colocalized with PINK1 on mitochondria (fig. S4A). In contrast, in the absence of toxin treatment, the cells appeared to accumulate less iCP-Parkin (fig. S4N), and the protein remained evenly distributed in the cytoplasm (fig. S4A). In addition, iCP-Parkin accumulates 2.1- and 2.9-fold in damaged mitochondria of Parkin WT and KO cells, respectively (Fig. 3, C and D). iCP-Parkin increased the ubiquitination of mitochondrial Rho guanosine triphosphatase (GTPase) 2 (Miro2) and other various mitochondrial Parkin substrates (Fig. 3E and fig. S4, B and C) and promoted mitophagy as assessed by biomarker expression (Fig. 3, F and G). Compared with the vehicle group, mitophagy staining was increased by two- and four-fold in the CCCP only and iCP-Parkin–cotreated group, respectively (Fig. 3G). However, an enzymatically inactive iCP-Parkin mutant [C444S (point-mutated variant from a catalytic cysteine at position 444 to serine) equivalent to the catalytically inactive C431S mutant of native Parkin] failed to ubiquitinate the Parkin substrate (fig. S4, D and E) and did not stimulate mitophagy in CCCP-treated cells (fig. S4F).

Cytoprotection by iCP-Parkin was associated with enhanced levels of mitochondrial proteins, including cytochrome c oxidase I (COX1), succinate dehydrogenase complex flavoprotein subunit A (SDH-A; Fig. 3H), translocase of the outer membrane mitochondrial import receptor subunit 20 (Tom20), translocase of the inner membrane 23 (Tim23), mitofusin 1 and 2 (MFN1 and MFN2), compared with the reduced levels seen in CCCP-treated cells (fig. S4H), and the effect required an aMTD domain (fig. S4G). iCP-Parkin also increased the ubiquitination of Parkin-interacting substrate (PARIS) and the expression of genes involved in mitochondrial biogenesis: peroxisome proliferator–activated receptor gamma coactivator 1α (PGC-1α), transcription factor A, mitochondrial (TFAM), and nuclear respiratory factor 1 and 2 (NRF1 and NRF2; Fig. 3I and fig. S4I). These results suggest that iCP-Parkin promotes mitochondrial biogenesis in toxin-treated cells.

On a cellular level, CCCP and 1-methyl-4-phenylpyridinium (MPP) induced dose-dependent increases in reactive oxygen species (ROS), reduced ATP levels, and increased apoptosis that were recovered by iCP-Parkin (Fig. 3, J to L, and fig. S4, J and K) in a dose-dependent manner (fig. S4L) and were accompanied by the expected changes in proapoptotic (p53, cytochrome C, and cleaved caspase-3) and antiapoptotic (Bcl2) biomarkers (fig. S4M).

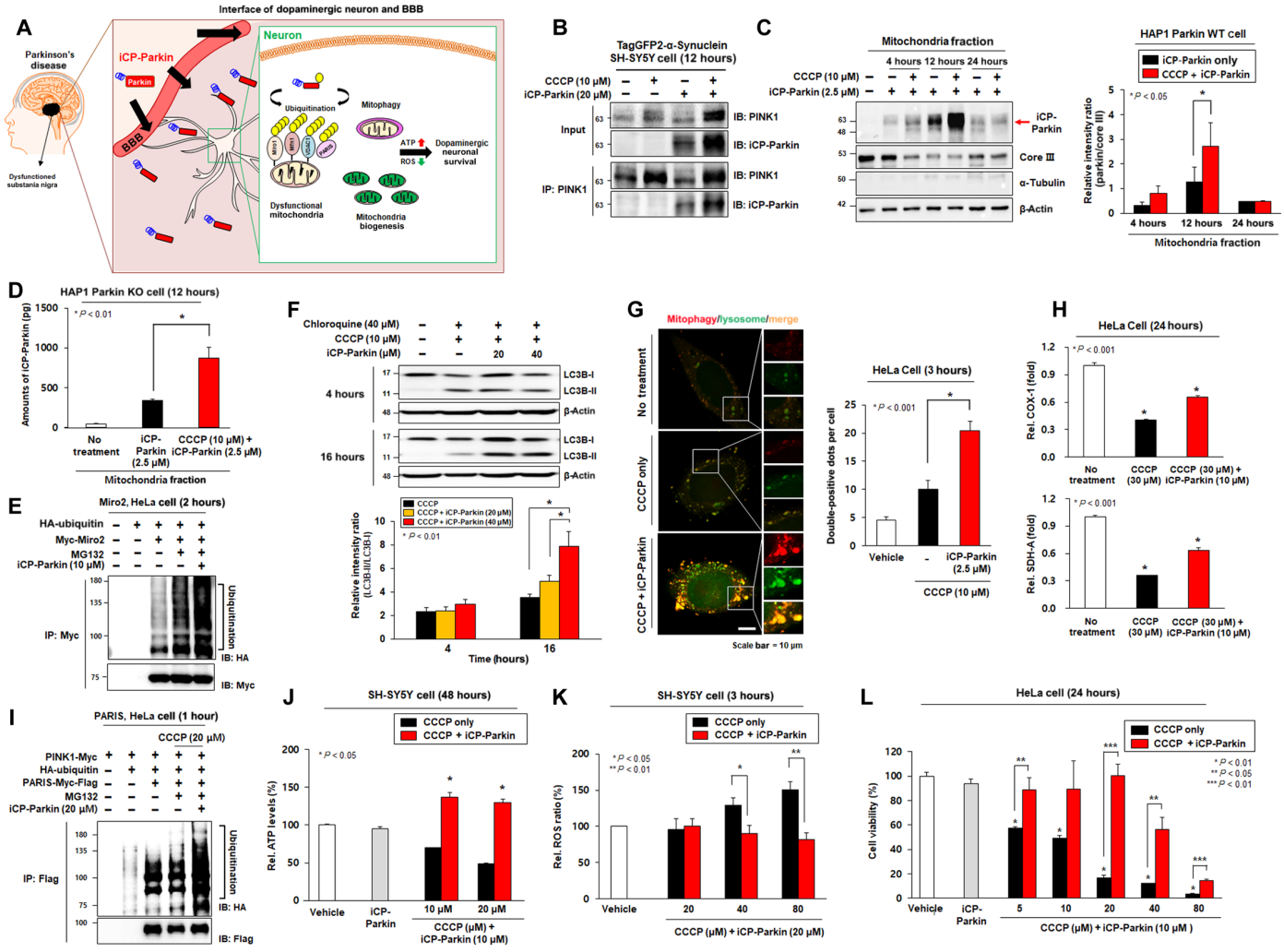

Fig. 3. iCP-Parkin promotes mitophagy and mitochondria biogenesis in toxin-treated cells. (**A**) Cytoprotective action mechanism of iCP-Parkin by promoting mitophagy and mitochondria biogenesis. (**B**) Immunoprecipitation (IP) assay for analyzing the interaction between PINK1and iCP-Parkin after CCCP treatment in TagGFP2–α-synuclein–SH-SY5Y cells. The representative data are presented, and the tests were carried out with three repetitions. IB, immunoblot. (**C**) Mitochondria were isolated from HAP1 Parkin WT cells treated with CCCP for 4, 12, and 24 hours. Western blot analysis was performed to detect iCP-Parkin. The level of iCP-Parkin was significantly increased in CCCP-treated mitochondria compared with normal mitochondria ($n = 3$). (**D**) Mitochondria were isolated from Parkin KO HAP1 cells treated with CCCP for 12 hours for ELISA. The amount of iCP-Parkin was significantly increased in the CCCP-treated group ($n = 3$). (**E**) Immunoprecipitation and Western blot analysis for analyzing the ubiquitination of Miro2 by iCP-Parkin using cell lysates from HeLa cells transfected with the indicated constructs and treated with CCCP and MG132 (20 μM each) for 6 hours in the presence or absence of iCP-Parkin. (**F**) Western blot analysis for detecting LC3B-II, an autophagy marker, in lysates from CCCP- or CCCP + iCP-Parkin–treated SH-SY5Y cells treated with chloroquine, an autophagy inhibitor. For quantification, the band intensity ratio of LC3B-II/LC3B-I in each group was normalized to that in the untreated control group ($n = 3$). (**G**) Representative confocal microscope images for detecting mitophagy increased by iCP-Parkin under CCCP treatment in HeLa cells ($n = 19$). (**H**) ELISA of the levels of mitochondrial proteins, COX1, and SDH-A in HeLa cells treated with either 30 μM CCCP or 10 μM iCP-Parkin as indicated ($n = 4$). Statistical comparisons were performed using Student's *t* test. (**I**) Immunoprecipitation and Western blot analysis for analyzing the ubiquitination of PARIS by iCP-Parkin using cell lysates from HeLa cells transfected with the indicated constructs and treated with CCCP and MG132 (20 μM each) in the presence or absence of i iCP-Parkin. (**J**) ATP levels were analyzed by an ATP Glo assay after cotreating SH-SY5Y cells with CCCP and Parkin recombinant proteins. iCP-Parkin recovered the ATP levels decreased by CCCP in a dose-dependent manner ($n = 3$). *$P < 0.05$ versus CCCP only. (**K**) iCP-Parkin also recovered the cellular ROS levels decreased by CCCP ($n = 3$). (**L**) Cell viability analysis using the CCK-8 assay in HeLa cells ($n = 3$). *$P < 0.01$ versus vehicle; **$P < 0.05$ versus CCCP only; ***$P < 0.01$ versus CCCP only. Scale bar, 10 μm. Data in (C), (D), (G), (H), (J), (K), and (L) are the means ± SEM with Student's *t* test. Data in (F) are represented as the means ± SEM, and statistics were analyzed by one-way ANOVA with post hoc Tukey's test analysis.

iCP-Parkin suppresses α-synuclein accumulation

Sporadic PD is associated with structures known as Lewy bodies that contain pathological (oligomeric, filamentous, or phosphorylated) forms of α-synuclein, α-synuclein–interacting protein, synphilin-1, and Pael-R (G protein–coupled receptor 37) (*20*–*23*). To study the effects of iCP-Parkin on α-synuclein aggregation, we used SH-SY5Y cells engineered to overexpress a green fluorescent protein (GFP)–tagged α-synuclein protein (designated TagGTP2-α-synuclein SH-SY5Y). Mitochondrial poisons, such as sodium arsenite and rotenone, stimulate the accumulation of insoluble, pathological forms of α-synuclein (*24*), as we also observed (Fig. 4 and fig. S5); moreover, the process was suppressed by iCP-Parkin. Oligomeric and filamentous α-synuclein were significantly decreased by 93 and 80% in the soluble fraction (Fig. 4B). iCP-Parkin significantly reduced pSer^{129}-α-synuclein,

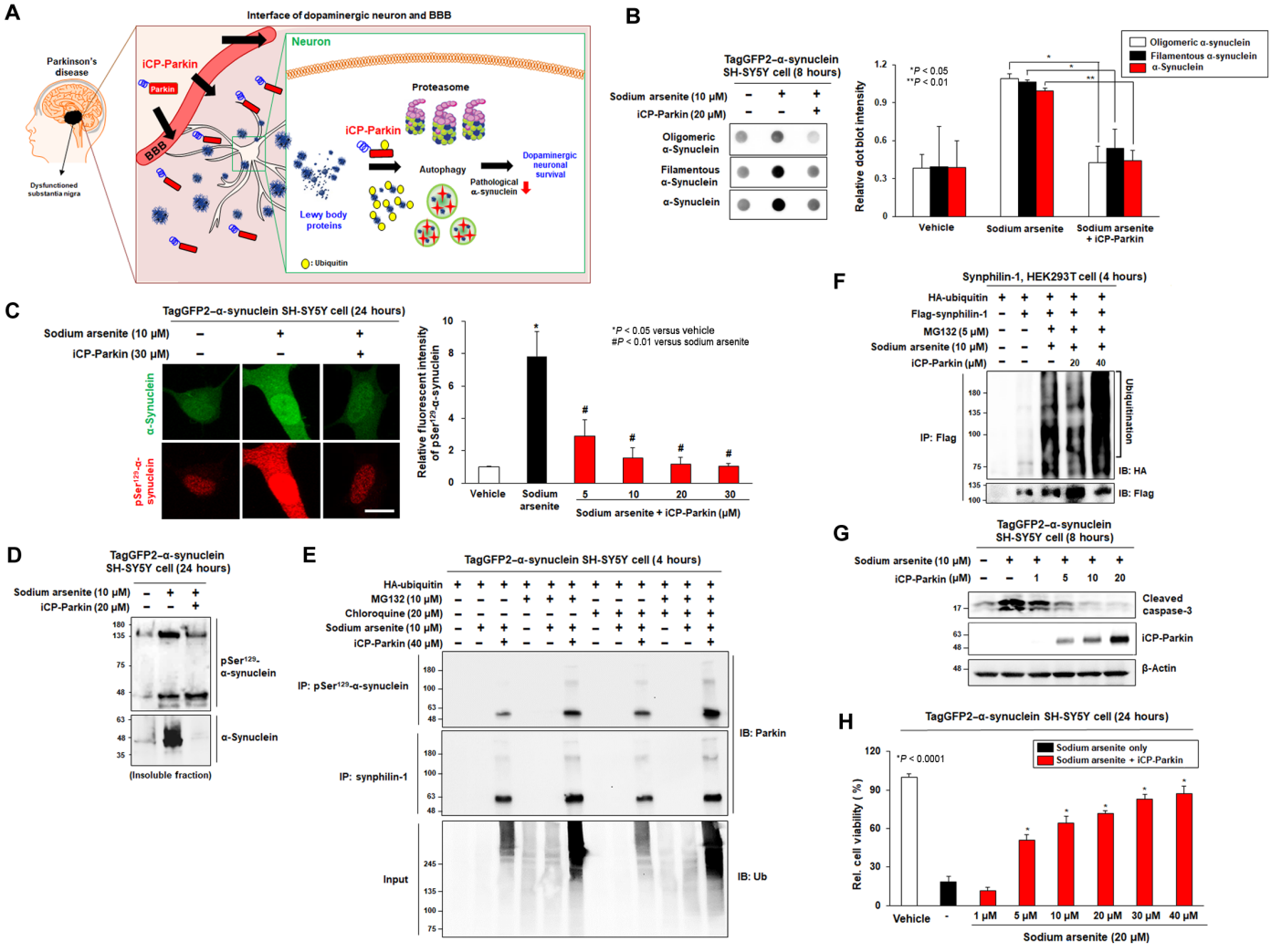

Fig. 4. iCP-Parkin suppresses the accumulation of pathological α-synuclein and has cytoprotective function in vitro. (**A**) Cytoprotective action mechanism of iCP-Parkin by reducing Lewy body proteins including pathological α-synuclein. (**B**) Representative dot blot images showing a significant decrease in pathological α-synuclein forms, such as oligomeric and filamentous, and α-synuclein by iCP-Parkin in the soluble fraction at 8 hours ($n = 3$). (**C**) Immunofluorescence imaging of phosphorylated ($pSer^{129}$) α-synuclein (p-α-synuclein; denoted as red colorized signal). iCP-Parkin reduced p-α-synuclein aggregates induced by treatment with sodium arsenite. The green fluorescent signal indicates GFP-tagged α-synuclein. The relative pixel intensity of the green fluorescent signal indicating a local concentration of GFP-tagged α-synuclein protein was quantified using ImageJ software. The graph demonstrates semiquantification of the relative fluorescence intensity in images indicating p-α-synuclein–positive signals. Scale bar, 10 μm ($n = 3$). (**D**) Representative Western-blotted image showing the reduction in neurotoxin-induced phosphorylated ($pSer^{129}$) α-synuclein and α-synuclein aggregates in the insoluble fraction by iCP-Parkin (20 μM). The representative data are presented, and the tests were carried out with three repetitions. (**E**) Immunoprecipitation assay with the soluble fraction demonstrating physical interactions between iCP-Parkin and phosphorylated ($pSer^{129}$) α-synuclein or synphilin-1 in TagGFP2–α-synuclein–SH-SY5Y stable cells (4 hours). Note that the same cell lysates were used for immunoprecipitation and input immunoblot simultaneously. Global ubiquitination was also increased by iCP-Parkin. The representative data are presented, and the tests were carried out at various time points (2 to 8 hours). (**F**) Immunoprecipitation assay for ubiquitination of synphilin-1 by iCP-Parkin in HEK293T cells. The representative data are presented, and the tests were carried out with two repetitions. (**G**) Western blot analysis showing a dose-dependent decrease in cleaved caspase-3 by iCP-Parkin at 8 hours. (**H**) CellTiter-Glo analysis showing a dose-dependent increase in cell viability by iCP-Parkin at 24 hours. Cell viability was analyzed using CellTiter-Glo analysis after cotreating the cells with different doses of iCP-Parkin and 20 μM sodium arsenite. *$P < 0.0001$ versus sodium arsenite only. Data in (B), (C), and (H) are expressed as the means ± SEM with Student's t test ($n = 3$).

which was induced by treatment with sodium arsenite or rotenone, in both immunostaining (Fig. 4C) and Western blot analysis (Fig. 4D and fig. S5, I and J), as well as total α-synuclein. In addition, iCP-Parkin significantly decreased apoptosis in sodium arsenite–treated cells (fig. S5, D and E). However, the C444S mutant failed to decrease pathological forms of α-synuclein (fig. S5, F and H, also in the test using non–CP-Parkin) and did not inhibit apoptosis and cytotoxicity levels (fig. S5, E and G), presuming that iCP-Parkin has a cytoprotective action by using both enzymatic activity as an E3 ubiquitin ligase and cell permeability.

iCP-Parkin physically interacted with $pSer^{129}$-α-synuclein and synphilin-1 in sodium arsenite–treated TagGTP2-α-synuclein SH-SY5Y cells, as assessed by coimmunoprecipitation concomitant with increases in total ubiquitination (Fig. 4E). In addition, iCP-Parkin enhanced substrate ubiquitination in cells overexpressing denoted substrates such as Pael-R and synphilin-1 (Fig. 4F and fig. S5, A and B).

Last, iCP-Parkin suppressed the toxicity of sodium arsenite in a dose-dependent manner with concomitant reductions in cleaved caspase-3, an apoptosis mediator (Fig. 4G). Furthermore, iCP-Parkin treatment showed dose-dependent cytoprotective activity against sodium arsenite in TagGTP2-α-synuclein SH-SY5Y cells (Fig. 4H). The ability of iCP-Parkin to suppress poison-induced accumulations of pathological forms of α-synuclein was sensitive to both proteasome [*N*-carbobenzyloxy-L-leucyl-L-leucyl-L-leucinal (MG132)] and autophagy (bafilomycin A1) inhibitors (fig. S5, C, K, and L), implicating that the ubiquitin proteasome system and autophagy-lysosome pathway systems are related to iCP-Parkin action (Fig. 4A).

Efficacy of iCP-Parkin in toxin-induced PD animal models

The neuroprotective activity of iCP-Parkin was tested in a 6-hydroxydopamine (6-OHDA)–induced PD mouse model (*25*). Saline or 4 μg of 6-OHDA was stereotaxically injected into the right medial forebrain bundle (MFB; day 0), and iCP-Parkin (30 mg/kg) or non–CP-Parkin was administered on days 4, 5, and 6 (Fig. 5A). 6-ODHA induced significant motor impairment (>60-fold) after 3 days compared with control groups based on the rotation test (Fig. 5B), and motor test was carried out on days 0 and 5 to 9 using the pole test. iCP-Parkin treatment led to steady improvements in descent times (to 82 and 71% of the control groups by days 8 and 9, respectively; whereas non–CP-Parkin had no effect Fig. 5C). Motor impairment was accompanied by repression of TH expression that was partially restored (74% recovery) by iCP-Parkin expression in the injected hemisphere as compared with the uninjected, contralateral side (Fig. 5, D to F). TH, the rate-limiting enzyme in DA biosynthesis, correlates with DA expression and provides a marker for dopaminergic neurons. More frequent administrations of iCP-Parkin (three times per week compared with once a week) further restored TH expression but without further improvements in motor function (fig. S6, A to C).

Considering the role of Parkin in mitophagy and mitochondrial biogenesis, we tested whether mitochondrial protein levels changed in response to 6-OHDA and iCP-Parkin treatment. As shown in fig. S6D, the levels of COX4 and voltage-dependent anion channel 1 (VDAC1) were reduced in the 6-OHDA–induced PD model and mitigated by iCP-Parkin treatment. These results suggest that the normal cellular Parkin-mitophagy pathway is overwhelmed by 6-OHDA–induced mitochondrial damage, and iCP-Parkin reinforces the Parkin-mitophagy response.

Similar studies examined the effectiveness of iCP-Parkin in the 6-OHDA rat PD model (*26*). iCP-Parkin (5, 15, or 30 mg/kg) was intravenously administered three times per week for 4 weeks starting on the third week after unilateral 6-OHDA injection into the striatum (Fig. 5G). PD disease induction was confirmed by using the rotation test, where 6-ODHA–injected animals showed significant motor deficits (more than 400-fold) compared with the diluent group (Fig. 5H). Motor deficits were recovered by iCP-Parkin in a dose-dependent manner (46, 77, and 100% compared with controls) (Fig. 5I). TH expression (Fig. 5J) and plasma DA levels (Fig. 5K) both declined in 6-OHDA–lesioned rat, while TH expression was largely restored in the striatum and substantia nigra (80 and 66%, respectively) by iCP-Parkin treatment (Fig. 5, L and M) along with improvements in motor function (89%). By contrast, motor functions in mice treated with cell-permeable C444S Parkin mutant protein continued to decline (by 20%) by the rotarod test (fig. S6, E and F).

Similar anti-Parkinsonian effects were also observed in mice treated with the mitochondrial poison MPTP and iCP-Parkin under a variety of conditions (fig. S7, A, E, H, and K). In all cases, iCP-Parkin treatment led to significant recovery of motor deficits as assessed by the gait [90% (stride) and 79% (sway); fig. S7B], swim (51%; fig. S7D), wire (86%; fig. S7J), and rotarod tests (93%; fig. S7L). Motor recovery was accompanied by 83% recovery of urine DA levels (fig. S7C) and restoration of TH expression (fig. S7, F, G, and I).

Efficacy of iCP-Parkin in α-synuclein–induced PD mouse model

Because α-synuclein is linked to sporadic PD, the most common presentation of the human disease (*27*), iCP-Parkin was tested in an α-synuclein–induced PD mouse model. Mice infected intracranially with an adeno-associated virus (AAV) α-synuclein expression vector experienced accumulations of soluble and insoluble α-synuclein forms after 4 weeks and 82% loss of DA-expressing neurons in the substantia nigra by week 8 (*27*). In our study, the infected mice began to show motor deficits 5 weeks postinitiation, and the defects became prominent by week 8 (Fig. 6 and fig. S8), indicative of late-early to middle-stage PD pathology.

Mice treated with iCP-Parkin (30 mg/kg, three times weekly for 4 weeks starting at week 8; Fig. 6A) displayed improved motor function as assessed by the rotarod test even in the first week, and their motor function improved to 90% of unlesioned controls by treatment week 4 (Fig. 6B). Motor deficits were accompanied by loss of TH-positive neurons in the substantia nigra, and these losses were abrogated by iCP-Parkin (Fig. 6C), which was also observed by immunostained sections of the striatum (fig. S8B). Furthermore, iCP-Parkin reduced α-synuclein levels in TH^+ neurons by 72 and 79% in the substantia nigra and the striatum, respectively (Fig. 6, D and E), consistent with the response observed in NeuN-positive cells (a pan-neuronal marker; fig. S8, C and E). In another test (Fig. 6, F to M) with a different protocol (10 mg/kg, three times per week), iCP-Parkin treatment led to progressive recovery of motor function (31, 54, and 72% at 9 to 11 weeks, respectively) in the pole test (Fig. 6G). TH expression was significantly recovered (63%), and α-synuclein was significantly decreased (68%) by Western blot analysis (Fig. 6H), consistent with immunostaining data (Fig. 6I).

Protein aggregates visualized by thioflavin S staining were also significantly reduced (76%) in the substantia nigra (Fig. 6J), also similarly observed in the striatum (fig. S8D), and reduced the levels of pathological [filamentous/aggregated (Fig. 6K and fig. S8H) and phosphorylated (Fig. 6, L and M)] α-synuclein and glial fibrillary acidic protein (GFAP; fig. S8G) in the striatum and/or substantia nigra regions. In addition, when iCP-Parkin (30 or 50 mg/kg, one time at 8 weeks) was administered after the injection of AAV–α-synuclein to the right side of the brain, iCP-Parkin recovered behavior defects by 100% in the beam test (fig. S6, G and H).

DISCUSSION

Mechanism-based drug development requires unambiguous evidence of therapeutic action consistent with targeting known biochemical pathways or associated molecular partners. PD poses several significant challenges to this drug discovery paradigm: (i) The underlying disease mechanism(s) is not well understood, (ii) existing animal models do not fully restage the pathophysiology of sporadic PD, and (iii) the disease is diagnosed after the onset of motor symptoms, at which point it is not clear if PD progression can be halted or reversed.

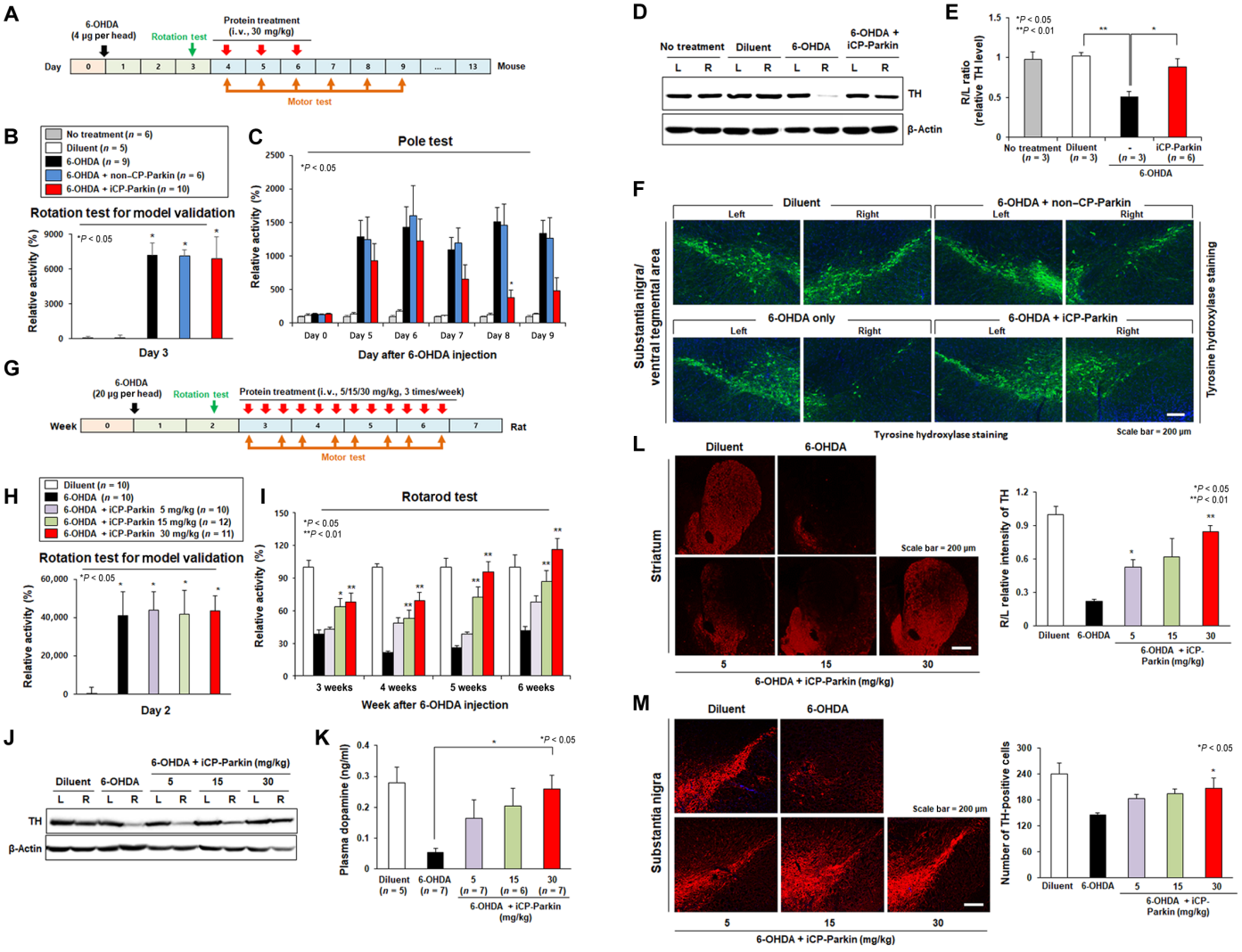

Fig. 5. iCP-Parkin ameliorates behavioral and molecular defects in 6-OHDA–induced PD animal models. (**A** to **F**) Efficacy of iCP-Parkin in a 6-OHDA–induced PD mouse model. (A) Schematic diagram of the experimental protocol. 6-OHDA (4 μg per head) was injected into the right side of the MFB. (B) Rotation test for confirming PD modeling at 3 days after 6-OHDA unilateral injection. (C) Pole test. After measuring the time to climb down a pole, raw data were converted into relative behavior activity based on the time of untreated control as 100%. *P < 0.05 versus 6-OHDA only. (D and E) Western blot analysis of TH expression (D) and graph of relative TH expression quantified using ImageJ (E) [n = 3, except iCP-Parkin (n = 6)]. Samples were collected 13 days after 6-OHDA treatment. L and R indicate the left and right sides of the brain, respectively. (F) Representative fluorescence imaging of TH expression in the substantia nigra. The fluorescence-based immunohistochemistry was performed to detect TH-positive dopaminergic neurons in the substantia nigra/ventral tegmental area. Scale bar, 200 μm (n = 3). (**G** to **M**) Efficacy of iCP-Parkin in a 6-OHDA–induced PD rat model. (G) Schematic diagram of the experimental protocol. Different doses of iCP-Parkin were intravenously injected three times per week for 4 weeks from 2 weeks after injecting 6-OHDA into the striatum on the right side of the brain. (H) Rotation test for confirming PD modeling at 2 weeks after 6-OHDA unilateral injection. (I) Rotarod test. Relative behavior activity is based on the value of the diluent control as 100% (n = 10 to 12). *P < 0.05 versus 6-OHDA only; **P < 0.01 versus 6-OHDA only. (J) Western blot analysis of TH expression. L and R indicate the left and right sides of the brain (n = 4). (K) Recovery of plasma dopamine levels by iCP-Parkin, as determined by ELISA. (L) TH expression in the striatum as assessed by fluorescence immunostained brain sections. The graph indicates the relative R/L ratios of fluorescence intensity compared with the R/L ratio in unlesioned (diluent) animals (set to 1). Scale bar, 200 μm (five to seven sections per animal, n = 5). *P < 0.05 versus 6-OHDA only; **P < 0.01 versus 6-OHDA only. (M) Fluorescence immunohistochemistry for detecting TH^+ dopaminergic neurons in the substantia nigra. The graph indicates stereological counting of TH^+ dopaminergic neurons in the substantia nigra. Scale bar, 200 μm. *P < 0.05 versus 6-OHDA only. Data in (B), (C), (H), and (I) are the means ± SEM. Data in (E), (L), (K), and (M) are the means ± SD. The P values were analyzed by one-way ANOVA with post hoc Tukey's test.

The present study describes advances in each of these areas. Specifically, we developed sequence-optimized aMTDs to enable efficient systemic delivery of protein therapeutics. The technology was used to evaluate Parkin as a potential drug in the treatment of PD. Intracellular delivery of iCP-Parkin into DA neuronal cells in vitro or in vivo suppressed neuronal toxicity by removing damaged mitochondria and/or reducing pathological α-synuclein. In addition, TH-positive cells in the striatum and the midbrain were restored, DA expression was enhanced, and gross motor function was recovered. This outcome suggests that Parkinsonian motor deficits may be reversible and that iCP-Parkin has therapeutic potential as a PD-modifying agent, which may overcome the critical limitation of PD symptom–relieving drugs such as L-3,4-dihydroxyphenylalanine (L-DOPA).

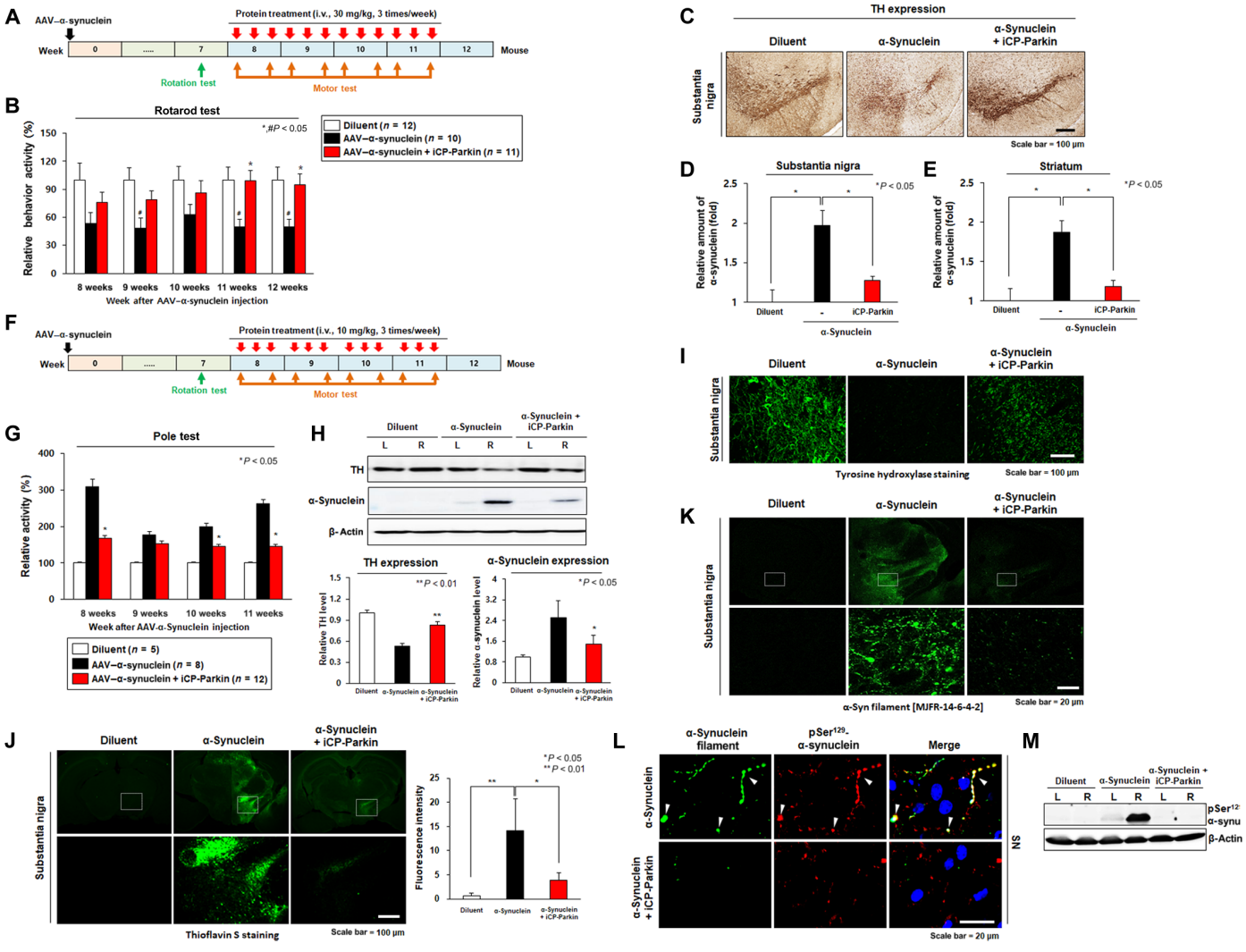

Fig. 6. iCP-Parkin recovers behavioral and biochemical defects in AAV–α-synuclein–induced PD animal models. (**A**) Schematic diagram of the experimental protocol in the AAV–α-synuclein–induced PD mouse model. iCP-Parkin (30 mg/kg) was intravenously injected three times per week for 4 weeks from 8 weeks after injecting AAV–α-synuclein into the right side of the brain (A to E). (**B**) Rotarod test. After recording the time walking on the rod, raw data were converted into relative behavior activity based on the time of diluent group as 100% ($n = 10$ to 12). #$P < 0.05$ versus diluent; *$P < 0.05$ versus AAV-α-Synuclein only. (**C**) Dopaminergic neurons were reduced in the group injected with AAV–α-synuclein compared with the normal group and confirmed the protection of dopaminergic neurons increased in the group injected with iCP-Parkin in the substantia nigra. Scale bar, 100 μm. (**D** and **E**) Quantitative graphs showing the relative fold change of α-synuclein level in the substantia nigra (left) and the striatum (right) measured by using ELISA ($n = 7$). (**F**) Schematic diagram of the experimental protocol in the AAV–α-synuclein–induced PD mouse model. iCP-Parkin (10 mg/kg) was intravenously injected three times per week for 4 weeks from 8 weeks after injecting AAV–α-synuclein into the right side of the brain (F to M). (**G**) Pole test. After measuring the time to climb down a pole, raw data were converted into relative behavior activity based on the time of the untreated control group as 100%. The data are presented as the means ± SEM, and the *P* values were determined by a post hoc Tukey's test after one-way ANOVA. The number sign (#) and asterisks (*) indicate comparisons between diluent and AAV–α-synuclein and between AAV–α-synuclein and AAV–α-synuclein with iCP-Parkin, respectively. *$P < 0.05$ versus AAV-α-Synuclein only. (**H**) Western blot analysis of TH and α-synuclein ($n = 3$). (Graph on left): **$P < 0.01$ versus AAV-α-Synuclein only. (Graph on right): *$P < 0.05$ versus AAV-α-Synuclein only. (**I**) Immunohistochemistry for detecting TH expression levels in substantia nigra. Scale bar, 100 μm. (**J**) Confocal laser scanning microscopy of thioflavin S–stained sections from the substantia nigra ($n = 3$). (**K**) Immunohistochemistry for detecting the expression levels of filamentous α-synuclein in substantia nigra. (**L**) Fluorescence coimmunohistochemistry and confocal laser scanning microscopy showing α-synuclein filament aggregate and pSer^{129}-α-synuclein in the substantia nigra. Note that iCP-Parkin significantly removes pSer^{129}-α-synuclein^{+} α-synuclein filament aggregates. Arrowheads demonstrate two signal double-positive α-synuclein species. Scale bar, 20 μm. (**M**) Western blot analysis for detecting pSer^{129}-α-synuclein in brain samples. The representative data are presented ($n = 3$). The level of pSer^{129}-α-synuclein increased by α-synuclein overexpression was significantly eliminated by iCP-Parkin administration. Data in (B), (D), (E), (G), (H), and (J) are the means ± SEM, and statistics were analyzed by one-way ANOVA with post hoc Bonferroni test.

Other hydrophobic sequences have been empirically found to enhance the delivery of protein cargos, including Parkin, into cells. However, the prior technology that suffered from two limitations is now addressed by TSDT. First, we identified six critical sequence motifs (critical factors) that, when satisfied by an aMTD sequence, enhanced protein delivery by an average of 13-fold compared with previous nonoptimized sequences. Second, protein SDs were used to enhance recombinant protein solubility. In all, aMTD development tested 19 aMTD sequences and 2 SDs—a process we have found to be effective in developing other cell-permeable proteins.

Four of the critical factors—length, hydrophobicity, α-helical moment, and internal proline—provide unbiased support for a mechanism of protein uptake suggested by structural studies of membrane-spanning peptides and biophysical interactions between peptides and model membranes (*28*, *29*). Briefly, the 12–amino acid aMTDs are predicted to adopt shorter, bent confirmations in an aqueous environment (due to an internal proline and the tilt angle between amino acids) and a longer, more linear conformation after insertion into the hydrophobic environment of the lipid bilayer (due to reduced helix bending by proline and increased tilt angles). The lengthening should then increase hydrophobic mismatch and favor exit from the membrane, presumably in either direction. Consistent with this model, aMTD-mediated protein uptake appeared to involve direct membrane penetration. Uptake did not require ATP, cell surface proteins, microtubule function, or endocytosis, but it required an intact and fluid membrane. Last, cell-to-cell transfer of iCP-Parkin implies bidirectional transport across the plasma membrane, consistent with a direct penetration model. Bidirectional transport would also account for extensive tissue penetration by iCP-Parkin in vivo, including the ability to cross the BBB. The current study demonstrating the neuroprotective effect of iCP-Parkin in deep brain including the striatum was achieved by the BBB permeability of iCP-Parkin, as well as in vivo systemic delivery, which was confirmed by a wide spectrum of quantitative and qualitative methodologies including LC-MS/MS, Western blot, ELISA, and cell-specific immunostaining of various brain regions.

A key challenge in medicine is the development of therapeutic agents with the desired activity, specificity, and bioavailability. In principle, therapeutic proteins have two advantages compared with conventional small-molecule drugs. First, the proteins interact across larger surfaces and, therefore, have greater specificity and fewer off-target effects. Second, whereas protein-protein interactions have been evolutionarily optimized, many proteins may not be "druggable" because they lack of small-molecule binding sites capable of producing the desired changes in protein activity.

The addition of an aMTD sequence greatly extended the persistence of recombinant Parkin and GFP proteins in vivo. We speculate that intracellular proteins transferred from cell to cell are sequestered from the blood and, therefore, are not excreted as rapidly as cell-impermeable, blood-borne proteins. aMTD sequences may provide an effective means to extend the half-lives of other therapeutic proteins, even proteins (e.g., antibodies) that do not require intracellular delivery. We show that the TSDT platform can be used to deliver Parkin protein systemically with a wide tissue distribution like most small-molecule drugs. Even so, iCP-Parkin became concentrated in the vicinity of damaged mitochondria, suggesting that the protein may be selectively retained in cells where it is biochemically engaged. This mechanism-specific cell targeting could help explain why iCP-Parkin, like Parkinson protein 2 (PARK2) transgenes, appear to be well-tolerated despite widespread tissue distribution.

iCP-Parkin appeared to be in a constitutively active, open conformation, either as a result of the refolding step during purification or by the attachment of the amino-terminal aMTD sequence (*15*). Nevertheless, iCP-Parkin recapitulated features of endogenous Parkin in the damage-induced mitophagy pathway (*30*). Internalized iCP-Parkin, colocalized with both PINK1 and mitochondria undergoing mitophagy, increased the ubiquitination of mitochondrial Parkin substrates and suppressed apoptosis induced by mitochondrial poisons. This suggests that iCP-Parkin reinforces endogenous cellular Parkin levels that are otherwise insufficient to protect cells against acute mitochondrial poisoning or the chronic damage associated with insoluble α-synuclein. Overall, the levels of cytoprotection achieved by iCP-Parkin were matched to those achieved by enforced PARK2 gene expression in both neuronal cell lines and transgenic animal models (*3*, *8*–*10*, *13*, *31*–*34*). However, the cytoprotective benefits of iCP-Parkin treatment were accrued within hours, even when the protein was delivered after cell damage.

In addition to removing damaged mitochondria by mitophagy (as evidenced by colocalization of mitochondria and lysosomes, and reduced levels of reactive oxygen, ATP, and mitochondrial proteins), iCP-Parkin enhanced mitochondrial biogenesis (based on increased ATP and mitochondrial protein levels). Once again, the behavior of iCP-Parkin was consistent with normal Parkin function, which is thought to promote mitochondrial biogenesis by ubiquitinating PARIS, a transcriptional repressor of PGC-1α, a coactivator of transcription factors, such as NRF1 and NRF2 (*35*, *36*). PINK1 interacts with and phosphorylates PARIS to regulate its ubiquitination and removal by Parkin (*36*). Likewise, PINK1 was required for PARIS ubiquitination by iCP-Parkin.

iCP-Parkin treatment reduced the levels of aggregated α-synuclein in cells by an unknown mechanism. Like Parkin, iCP-Parkin ubiquitinates synphilin-1 and Pael-R (but not α-synuclein), which are known Parkin substrates and accumulated in Lewy bodies together with α-synuclein (*22*, *23*). iCP-Parkin could influence Lewy body formation or clearance at the level of protein turnover. Alternatively, iCP-Parkin could suppress processes (e.g., mitochondrial dysfunction and/or ROS production) that generate pathological forms of α-synuclein or promote their aggregation.

Our results are consistent with a model in which mitochondrial poisons and aggregated α-synuclein suppress DA expression by down-regulating TH, the rate-limiting enzyme in DA biosynthesis. TH is subject to multiple levels of transcriptional and posttranscriptional regulation (*37*), and reversible loss of TH expression may function as a normal self-protective mechanism in times of neuronal stress. This would relieve dopaminergic neurons of the additional burden of endogenously produced and toxic DA metabolites [e.g., 1-methyl-6,7-dihydroxy-1,2,3,4-tetrahydroisoquinoline (salsolinol) and 3,4-dihydroxyphenylacetaldehyde; (*38*, *39*)], as illustrated by the ability of 6-OHDA to induce PD symptoms. The self-protection model implies that some loss of TH staining during PD progression may not initially be caused by neuronal death and therefore might be reversed. Together, this would provide a window of opportunity for therapeutic interventions to restore DA expression even after the onset of motor symptoms, as observed in animals treated with iCP-Parkin.

MATERIALS AND METHODS

Expression and purification of Parkin recombinant proteins

The optimized iCP-Parkin coding sequence was cloned into pET-26b(+) vector. The protein was expressed in *Escherichia coli* BL21-CodonPlus (DE3)-RIL cells using modified TB media (for 1 liter: 10 ml of glycerol, 24 g of yeast extract, 12 g of soy peptone, 9.4 g of K_2HPO_4, and 2.2 g of KH_2PO_4). The cells were grown to an OD_{600} (optical density at 600 nm) of 3 to 4 and induced for 3 to 4 hours with 0.5 mM isopropyl-β-D-thiogalactopyranoside (IPTG). Subsequently, the cells were harvested by centrifugation (8000 rpm, 4°C, 10 min) when OD_{600} value was approximately 12. Fermentation was done

using a 50-liter fermenter with agitation speed of 250 to 300 rpm and constant aeration rate of 0.5 aeration volume/media volume/minute (VVM) at 37°C. The harvested cells were disrupted by sonication (amplitude of 60%, 5-s sonication/5-s rest interval) for 30 min in lysis buffer {50 mM 3-[cyclohexylamino]-1-propanesulfonic acid (CAPS) (pH 10.5) and 1.0 M NaCl}. Afterward, inclusion body was isolated by centrifugation (2500*g* for 30 min at 4°C) and was washed one time with lysis buffer. The washed inclusion body was dissolved in unfolding buffer [8 M urea, 50 mM CAPS (pH 10.5), 0.5% CHAPS, and 10 mM dithiothreitol (DTT)] at room temperature (RT) for 1 hour. Then, the sample was incubated at RT for 3 hours with addition of 0.1 mM $ZnCl_2$. The unfolded protein was poured into refolding buffer [0.5 M arginine, 150 mM NaCl, 100 mM non-detergent sulfobetaines (NDSB), 50 mM tris, 2 mM reduced glutathione, 0.2 mM oxidized glutathione disulfide, and 1 mM DTT (pH 8.0)]. Once the refolding process was completed for 48 hours, ion exchange chromatography (IEX) was conducted as a capturing chromatography with the AKTA Purifier FPLC (fast protein liquid chromatography) System (GE Healthcare). Briefly, Q-Sepharose high-performance column was equilibrated and flowed with protein solution in equilibrium buffer [50 mM tris (pH 8.0), 0.1 M NaCl, and 1 mM DTT]. Subsequently, the column was washed with the equilibrium buffer and washing buffer [50 mM tris (pH 8.0), 0.17 M NaCl, and 1 mM DTT) to remove the unbound proteins. Then, the proteins were eluted with elution buffer [50 mM tris (pH 8.0), 0.35 M NaCl, and 1 mM DTT). After IEX chromatography, size exclusion chromatography was performed by using a Superdex 200. After the purification, the protein was concentrated using Pellicon 2 and Sartocon slice Ultrafiltration Unit (Sartorius). Endotoxin was removed using EndoTrap high-definition (HD) column (Hyglos GmbH). Last, proteins were dialyzed against a storage buffer [50 mM tris and 150 mM NaCl (pH 8.0)] using Sephadex G-25 column (GE Healthcare).

Analysis of protein uptake by cultured cells

Recombinant Parkin proteins were conjugated to 5/6-FITC according to the manufacturer's instructions (Sigma-Aldrich). SH-SY5Y cells were treated with 10 μM FITC-labeled recombinant proteins for 1 hour at 37°C, washed three times with cold phosphate-buffered saline (PBS), and treated with proteinase K (10 μg/ml) for 20 min at 37°C to remove surface-bound proteins, and internalized proteins were visualized by flow cytometry using a Guava easyCyte 8 instrument (Millipore).

C2C12 cells were treated with different agents to assess the mechanism of protein uptake, as follows: (i) proteinase K (10 μg/ml) for 10 min; (ii) 10 μM antimycin in the presence or absence of 1 mM ATP for 2 hours; (iii) 10 mM EDTA for 1 hour; (iv) incubation on ice (or at 37°C) for 15, 30, or 60 min; (v) 20 μM Taxol for 30 min; (vi) 5 mM amiloride for 30 min; (vii) 3 μM chlorpromazine for 30 min; and (viii) 5 mM methyl-β-cyclodextrin for 30 min. The cells were then incubated with 10 μM FITC-labeled proteins for 1 hour at 37°C, washed three times with ice-cold PBS, treated with proteinase K (10 μg/ml for 20 min at 37°C) to remove surface-bound proteins, and analyzed by flow cytometry.

To assess cell-to-cell protein transfer, donor C2C12 cells were treated with 10 μM FITC-conjugated iCP-Parkin and non–CP-Parkin proteins in serum-free DMEM medium for 2 hours at 37°C followed by washing, and mixed with mouse RAW264.7 cells (recipient cells) labeled with (PE) rat anti-mouse CD14 antibody (BD Biosciences, San Jose, CA) for 2 hours at 37°C in a 5% CO_2 incubator. Cell-to-cell protein transfer represented by FITC/PE double-positive cells, was monitored by a Guava easyCyte Benchtop Flow Cytometer (Millipore).

Primary neuronal culture and double immunocytochemistry

Institute of Cancer Research (ICR) pregnant females (13.5 days) were euthanized by cervical dislocation to isolate primary neurons. The isolated ventral mesencephalon from the fetuses was pooled, and single primary cortical neuronal cells were obtained by incubation with Accutase (Thermo Fisher Scientific) for 15 min at 37°C. Neurobasal medium (Thermo Fisher Scientific) containing L-glutamine, B-27 supplement (Thermo Fisher Scientific), B-27 plus supplement (Thermo Fisher Scientific), 10% fetal bovine serum (FBS), and ascorbic acid solution were used for cell culture. The cells were plated at a density of 1.5×10^4 cells/cm^2 in the poly-D-lysine/laminin-coated plates and further cultured at 37°C in a 5% CO_2 incubator for 7 days. For cell permeability test, primary neuron was seeded 0.5×10^5 per well in the 12-well plate. iCP-Parkin (10 μM) and 6-OHDA (30 μM; Sigma-Aldrich) were cotreated for 2 and 24 hours. For immunostaining, ß-III tubulin (Abcam, USA, catalog no. ab18207) and Parkin (Novus Biologicals, catalog no. NBP2-29838) antibodies were used as primary antibodies.

Systemic protein delivery of Parkin proteins to the brain and other tissues

Several methods were used to investigate the delivery of recombinant proteins to the brain and other tissues. (i) Delivery of FITC-conjugated proteins was visualized by fluorescence microscopy in cryosections (30 μm). Alternatively, minced tissues were passed through a 70-μm nylon cell strainer (BD Biosciences), and the cell suspensions were analyzed by flow cytometry with a Guava easyCyte instrument (Millipore). For immunostaining, MAP2 antibody (Abcam, ab32454) was used for detecting neurons. (ii) For Western blot analysis, tissue lysates were prepared after perfusion with PBS to remove residual blood within the tissues and stored at −80°C. (iii) Signature peptides from the aMTD segment of iCP-Parkin were detected by LC-MS/MS analysis of brain tissues [under contract with Envigo (Huntingdon, UK)]. Briefly, brain lysates were digested using two different digestion kits, SMART Digest (Thermo Fisher Scientific) and ProteinWorks (Waters), and peptides were separated on an ACE UltraCore SuperC18 column (Advanced Chromatography Technologies) with an acetonitrile gradient and analyzed on a Sciex API 6500+ mass spectrometer (SCIEX). Ions generated by the signature peptide carried charges of $(M+2H)2^+$ and $(M+3H)3^+$ and were detected at 940.4 and 627.4 Da, respectively. (iv) Last, levels of iCP-Parkin protein in the brain and serum were determined by an ELISA kit (KOMA BIOTECH). Horseradish peroxidase (HRP) reaction products were measured at 450 nm with a microplate reader (Synergy H1, BioTek Instruments).

Cells and antibodies related to in vitro mechanism studies

SH-SY5Y and TagGFP2-α-synuclein SH-SY5Y cells were commercially acquired (Innoprot). HAP1 and Parkin-KO human near-haploid (HAP)1 cells were obtained from the Horizon Discovery. NIH3T3, RAW264.7, and C2C12 cells were obtained from the American Type Culture Collection (ATCC). Cell viability was evaluated by CellTiter-Glo cell viability assay (Promega) and quantified using a luminometer (Turner Designs) or luminescence plate reader (Synergy H1, BioTek Instruments). Apoptosis was assayed by annexin V/7-aminoactinomycin D (7-AAD) staining as directed by the supplier (BD Biosciences) and analyzed by flow cytometry on a Guava easyCyte 8 instrument (Millipore). To visualize mitochondria and mitochondria undergoing mitophagy, cells were stained with 1 mM Lyso Dye (Dojindo Molecular Technologies) and 100 nM Mtphagy Dye (Dojindo Molecular Technologies),

respectively. Mitochondrial biogenesis was monitored by the Mito-Biogenesis In-Cell ELISA Kit (Abcam, ab110217). Measurements of intracellular ROS used the Abcam ROS detection kit (Abcam, ab113851).

Procedures for Western blot analysis and immunostaining of cells and tissues are described previously (*13*). Soluble and insoluble cell fractions were prepared as described elsewhere (*40*). For dot blot analysis, cell lysates (1.5 μg of protein) were bound to nitrocellulose membranes with a Bio-Dot microfiltration apparatus (Bio-Rad) by gravity filtration. This passive filtration is necessary for quantitative antigen binding.

The ability of iCP-Parkin to ubiquitinate or physically interact with specific proteins was studied by immunoprecipitation Western blot analysis in HeLa, human embryonic kidney (HEK) 293T, or SH-SY5Y cells transiently transfected with plasmids expressing HA-tagged human ubiquitin, Myc-Miro2 (Addgene, 47891), Myc-Flag-PARIS (OriGene, RC209784), Myc-PINK1 (Addgene, 13314), Myc-Mfn1 (Addgene, 23212), Myc-Mfn2 (Addgene, 23213), Flag-Peal-R (OriGene, Rc208054), or Flag-synphilin (GenScript, OHu19245D). Cells were transfected using Lipofectamine 3000 (Thermo Fisher Scientific) according to the manufacturer's instructions and were treated or not with mitochondrial poisons (sodium arsenite, Sigma-Aldrich) and iCP-Parkin depending on the experiment and lysed in IP lysis buffer [Thermo Fisher Scientific, 1% Triton X-100 in 1× PBS buffer (pH 7.4)] supplemented with EDTA-free protease inhibitor mix (Roche). Proteins, normalized by Bradford assay, were immunoprecipitated using the relevant antibodies. Immune complexes were recovered using Protein G Sepharose 4 Fast Flow (GE Healthcare) and analyzed by Western blot analysis.

Antibodies were purchased from the following sources and used as specified by the supplier: Novus Biologicals (Parkin, NBP2-29838, epitope: 399-465 A/a); Merck Millipore (Parkin, MAB5512; TH, A5152); Ubiquigent (pSer^{65}-Parkin); Cell Signaling Technology (PINK1, ab75487; LC3B, 2775; cleaved caspase-3, 9664; HA tag, 3724S; Myc tag, 2272; and HRP-conjugated anti-mouse secondary antibody, 7076S); Sigma-Aldrich (β-actin, A3854); ENZO Life Sciences (ubiquitin, BML-PW-8810-0500); BioLegend (PINK1, 846202); ABclonal (Abclone, SDB, clone 7C1); Thermo Fisher Scientific (anti-rabbit Alexa 488, A-11034; anti-chicken Alexa 568, A11041); Abcam (α-synuclein, ab138501; pSer^{129} α-synuclein, ab51253; GFAP, ab-53554); MBL Life Sciences (Myc tag, M192-3); and Vector Laboratories (biotinylated rabbit anti-rat, BA-1000). Proteins in Western blots were visualized by chemiluminescence (SuperSignal West Femto, Thermo Fisher Scientific) and scanned using a ChemiDoc instrument (Bio-Rad). MG132, a proteasome inhibitor, was added to some treatment groups to stabilize ubiquitinated proteins in the immunoprecipitation tests.

For in vitro studies relevant to pathological α-synuclein model, the TagGFP2-α-synuclein SH-SY5Y cell line was seeded, and iCP-Parkin protein at designated concentrations and durations was cotreated with a neurotoxin, sodium arsenite (10 or 20 μM). Inhibitors to block proteasome or autophagy inhibitors were used with designated concentrations as follows: proteasome (MG132) and autophagy (chloroquine or bafilomycin A1).

PD animal models

All in vivo experiments were performed in a blinded manner. Usually, one researcher would randomize the animals and slides, and another would analyze them. The following criteria were developed to remove any possible outliers from animal groups before treating iCP-Parkin; animals that did not recover from the surgery, exhibited more than 30% body weight loss, or had normal rotation test outcomes after inducing the PD model were excluded from the group for further analysis. All behavior tests were repeated three times per animal for each experimental date, and numerous different PD animal models were used for the iCP-Parkin efficacy study.

iCP-Parkin was tested in several animal models for the ability to prevent and/or restore PD-related motor symptoms. In each model, the onset of motor symptoms was verified by an apomorphine rotation test (*41*) before starting iCP-Parkin treatments. Animals were injected subcutaneously with apomorphine (0.1 mg/kg) (freshly dissolved in 0.1% ascorbic acid solution and kept on ice in the dark before use) and judged to be symptomatic if side-biased rotation of lesioned mice turns faster than a rate of ~60 turns over 20 min. Parkin proteins were administered intravenously at the times and doses as described in the text, and changes in motor function were monitored as described below.

6-OHDA–induced PD mouse model

C57BL/6 mice (9 to 13 weeks, male) were anesthetized by a 1:1 mixture of Zoletil:Rompun (Bayer) diluted 1:10 in saline, positioned onto a stereotaxic apparatus, and injected with 4 μg of 6-OHDA (Sigma-Aldrich) dissolved in 0.8 μl of 0.01% ascorbic acid (Sigma-Aldrich) at a rate of 0.2 μl/min into the MFB at the following coordinates (relative to the bregma): anterior-posterior (AP) = −1.2 mm, medial-lateral (ML) = −1.2 mm, and dorsal-ventral (DV) = −4.75 mm (from the dura) with a flat skull position. Control mice were injected with 0.01% ascorbic acid solution alone.

AAV–αAsynuclein–induced PD mouse model

Anesthetized C57BL/6 mice (8 weeks, male) were stereotaxically injected with the human WT α-synuclein AAV/DJ vector (1 μl of 1.4×10^{13} genome copies (GC)/ml titer; Research Animal Resource Center, KIST) at a rate of 0.5 μl/min into the substantia nigra at the following coordinates (relative to the bregma): AP = −3.1 mm, ML = −1.2 mm, and DV = −4.00 mm (from the dura) with a flat skull position. The control group was injected with saline.

6-OHDA–induced PD rat model

Anesthetized male Sprague-Dawley rats (~230 g) were injected with 20 μg of 6-OHDA (5 μg/μl) at a rate of 0.5 μl/min into the striatum at the following coordinates (relative to the bregma): AP = −1.0 mm, ML = −2.8 mm, and DV = −6.0, 5.5, 5.0, and 4.4 mm (from the dura) with a flat skull position. The control group was injected with 0.01% ascorbic acid solution.

Motor function analysis

Pole test

Mice were placed on the top of a vertical pole (50-cm length with 1-cm diameter). The time to descend to the floor was measured. The test was recorded with a maximum duration of 60 s and repeated three to five times per animal.

Rotarod test

Mice were pretrained on a rotarod apparatus at 15 rpm for 300 or 720 s to achieve stable performance. The test was conducted with a gradually accelerated speed from 4 to 40 rpm over a period of 300 s, and the time each mouse was able to stay on the rod was recorded. Each animal was tested three to five times.

Immunohistochemistry

Animals were deeply anesthetized with a Zoletil:Rompun mixture and were perfused with saline and 4% paraformaldehyde (PFA; BIOSESANG) for 15 to 20 min. Brains were quickly fixed with 4% PFA for 2 hours at 4°C, incubated with 30% sucrose (DAEJUNG) at 4°C for 48 hours,

and embedded with optimal cutting temperature (OCT) compound (Leica Biosystems), and cryosections (30-μm thickness) were cut. Endogenous peroxidase activity was blocked by incubating the sections with 3% H_2O_2 (DAEJUNG) in methanol for 15 min. After washing in PBS, sections were incubated with blocking solution (1.5% normal goat serum in PBS; Vector Laboratories, S-1000) for 30 min. Sections were incubated with rabbit polyclonal TH antibody (1:1000; Millipore, AB152) at 4°C for 24 hours, followed by biotinylated rabbit anti-rat immunoglobulin G (IgG; 1:200; Vector Laboratories, BA-1000) for 1 hour at room temperature; sections were subsequently treated with avidin-biotinylated peroxidase complex using an ABC Kit (Vector Laboratories, PK-6100) for 30 min at room temperature. The sections were then treated with 3,30-diaminobenzidine (DAB peroxidase substrate kit, Vector Laboratories) as a chromogen. Permanently mounted slides were observed and photographed using a microscope equipped with a digital imaging system (DS-Ri2, Nikon). For fluorescence immunohistochemistry (IHC), rabbit polyclonal TH antibody (Millipore, AB152), rabbit polyclonal α-synuclein filament (Abcam, ab209538), and anti-rabbit $pSer^{129}$-α-synuclein (GeneTex, GTX50222) antibodies were applied to sections with a 1:1000 dilution at 4°C for 24 hours. After rinsing with PBS, sections were incubated with anti-rabbit Alexa 488 secondary antibody (Thermo Fisher Scientific, A-11034) or anti-chicken Alexa 647 secondary antibody (Thermo Fisher Scientific, A-21449) at 1:2000 dilution for 1 hour at room temperature. Sections were mounted with 4′,6-diamidino-2-phenylindole (DAPI) mounting medium (Vector Laboratories, H-1200) and were observed and photographed using a confocal microscope equipped with a digital imaging system (TCS SP8-gSTED, Leica). To count TH^+ neurons in the substantia nigra, brain samples were dissected in three series. All three series were taken from levels −4.8 to −5.6 mm (from anterior to posterior) to bregma. Each section was cryo-sectioned with a thickness of 20 μm. Cells with a certain area of the fluorescent signal (serially detected with above 25 pixels in the binary black-white version of image) were judged to be TH^+ and were manually counted. We counted 150 to 350 cells (per section) for quantification.

Thioflavin S staining of α-synuclein aggregates

After defatting in xylene for 5 min and subsequently hydrating through a series of ethyl alcohol solutions (100, 95, 80, and 70%, 5 min in each), cryosections were stained with 1% Thioflavin S (in distilled water; Sigma-Aldrich) for 60 min. The sections were subsequently dehydrated through a series of ethyl alcohol solutions (70, 80, 95, 100, 100%, 5 min in each one) and then placed in xylene for 5 min before being coverslipped with mounting media. Permanently mounted slides were observed and photographed using a microscope equipped with a digital imaging system (DS-Ri2, Nikon).

Determination of plasma DA levels

Blood samples were collected with EDTA tubes (BD Biosciences) after behavior tests. The collected samples were centrifuged for 20 min at 13,000 rpm at 4°C within 30 min after sample collection and analyzed using an ELISA kit (Dopamine High-Sensitive ELISA, Eagle Bioscience Inc.) following the manufacturer's protocol.

Western blot analysis and ELISA for α-synuclein clearance in animal studies

To analyze α-synuclein clearance in brain samples, the isolated brains were homogenized in PRO-PREP lysis buffer (iNtRON Biotechnology) containing a protease inhibitor (Thermo Fisher Scientific). The quantified cell lysates were separated by 10% SDS–polyacrylamide gel electrophoresis (PAGE) and transferred to nitrocellulose membranes (Bio-Rad). Membranes were incubated with primary antibodies against α-synuclein (1:1000; Santa Cruz Biotechnology, SC-12767), TH (1:2000; Millipore, AB152), $pSer^{129}$-α-synuclein (1:5000; Abcam, ab51253), and β-actin (1:100,000; Sigma-Aldrich, A3854) followed by secondary antibodies. After visualization using SuperSignal West Dura (Thermo Fisher Scientific), immunoblots were quantified with ImageJ software. For ELISA, brain samples were collected after behavior tests. The collected samples were centrifuged for 20 min at 13,000 rpm at 4°C within 30 min after sample collection and analyzed using a commercially available α-synuclein ELISA kit (AnaSpec) following the manufacturer's direction.

Statistical analysis

The in vitro tests that were quantified in all graphs were independently performed with a minimum sample number of $n = 3$ per group for appropriate statistical analysis [t test or analysis of variance (ANOVA)] following data collection for all quantified data. We performed appropriate statistical analysis to demonstrate statistical significance between designated groups as numerous published data were presented (*42*). In addition, to confirm the significant findings (e.g., suppression of pathological α-synuclein), we cross-checked our meaningful data via repeated experiments with different toxins (e.g., sodium arsenite versus rotenone) at different time points using diverse analysis methods such as fluorescence imaging, Western blot, and fluorescence-activated cell sorting performed by several researchers. Statistical analyses were performed with GraphPad Prism or Excel software using Student's t test or one-way ANOVA. One-way ANOVA was followed by Tukey's or Bonferroni multiple comparisons test. $P < 0.05$ was considered statistically significant. Data are represented as the means ± SD or means ± SEM as indicated.

Ethics statement

Animal handling and experimental procedures were approved and performed in accordance with the guidelines of the Institutional Review Board of the Cellivery R&D Institute, Cellivery Therapeutics Inc. Male C57BL/6 mice on arrival were housed in groups of five to six in standard cages. Male Sprague-Dawley rats (~230 g) were housed in groups of three in standard cages. Animals were maintained under controlled temperature (22° ± 2°C) on a 12-hour dark/12-hour light cycle with free access to food and water. Two to three animals were accommodated per cage following surgery to prevent bullying and facilitate feeding.

SUPPLEMENTARY MATERIALS

Supplementary material for this article is available at http://advances.sciencemag.org/cgi/content/full/6/18/eaba1193/DC1

REFERENCES AND NOTES

1. J. M. Shulman, P. L. De Jager, M. B. Feany, Parkinson's disease: Genetics and pathogenesis. *Annu. Rev. Pathol.* **6**, 193–222 (2011).
2. H. Braak, K. Del Tredici, U. Rüb, R. A. I. de Vos, E. N. H. Jansen Steur, E. Braak, Staging of brain pathology related to sporadic Parkinson's disease. *Neurobiol. Aging* **24**, 197–211 (2003).
3. T. M. Dawson, V. L. Dawson, The role of parkin in familial and sporadic Parkinson's disease. *Mov. Disord.* **25** (Suppl 1), S32–S39 (2010).

4. H. Xiong, D. Wang, L. Chen, Y. S. Choo, H. Ma, C. Tang, K. Xia, W. Jiang, Z. Ronai, X. Zhuang, Z. Zhang, Parkin, PINK1, and DJ-1 form a ubiquitin E3 ligase complex promoting unfolded protein degradation. *J. Clin. Invest.* **119**, 650–660 (2009).
5. J. Park, S. B. Lee, S. Lee, Y. Kim, S. Song, S. Kim, E. Bae, J. Kim, M. Shong, J.-M. Kim, J. Chung, Mitochondrial dysfunction in *Drosophila PINK1* mutants is complemented by *parkin*. *Nature* **441**, 1157–1161 (2006).
6. D. Salat, A. J. Noyce, A. Schrag, E. Tolosa, Challenges of modifying disease progression in prediagnostic Parkinson's disease. *Lancet Neurol.* **15**, 637–648 (2016).
7. I. E. Clark, M. W. Dodson, C. Jiang, J. H. Cao, J. R. Huh, J. H. Seol, S. J. Yoo, B. A. Hay, M. Guo, *Drosophila pink1* is required for mitochondrial function and interacts genetically with *parkin*. *Nature* **441**, 1162–1166 (2006).
8. C. Lo Bianco, B. L. Schneider, M. Bauer, A. Sajadi, A. Brice, T. Iwatsubo, P. Aebischer, Lentiviral vector delivery of parkin prevents dopaminergic degeneration in an α-synuclein rat model of Parkinson's disease. *Proc. Natl. Acad. Sci. U.S.A.* **101**, 17510–17515 (2004).
9. L. Vercammen, A. Van der Perren, E. Vaudano, R. Gijsbers, Z. Debyser, C. Van den Haute, V. Baekelandt, Parkin protects against neurotoxicity in the 6-hydroxydopamine rat model for Parkinson's disease. *Mol. Ther.* **14**, 716–723 (2006).
10. T. Yasuda, H. Hayakawa, T. Nihira, Y. R. Ren, Y. Nakata, M. Nagai, N. Hattori, K. Miyake, M. Takada, T. Shimada, Y. Mizuno, H. Mochizuki, Parkin-mediated protection of dopaminergic neurons in a chronic MPTP-minipump mouse model of Parkinson disease. *J. Neuropathol. Exp. Neurol.* **70**, 686–697 (2011).
11. I. Martin, V. L. Dawson, T. M. Dawson, Recent advances in the genetics of Parkinson's disease. *Annu. Rev. Genomics Hum. Genet.* **12**, 301–325 (2011).
12. D. Jo, A. Nashabi, C. Doxsee, Q. Lin, D. Unutmaz, J. Chen, H. E. Ruley, Epigenetic regulation of gene structure and function with a cell-permeable Cre recombinase. *Nat. Biotechnol.* **19**, 929–933 (2001).
13. T. Duong, J. Kim, H. E. Ruley, D. Jo, Cell-permeable parkin proteins suppress Parkinson disease-associated phenotypes in cultured cells and animals. *PLOS ONE* **9**, e102517 (2014).
14. J. Kyte, *Structure in Protein Chemistry* (Garland Science, 2006).
15. L. Burchell, V. K. Chaugule, H. Walden, Small, N-terminal tags activate Parkin E3 ubiquitin ligase activity by disrupting its autoinhibited conformation. *PLOS ONE* **7**, e34748 (2012).
16. T. Kitada, S. Asakawa, N. Hattori, H. Matsumine, Y. Yamamura, S. Minoshima, M. Yokochi, Y. Mizuno, N. Shimizu, Mutations in the *parkin* gene cause autosomal recessive juvenile parkinsonism. *Nature* **392**, 605–608 (1998).
17. F. Darios, O. Corti, C. B. Lücking, C. Hampe, M. P. Muriel, N. Abbas, W.-J. Gu, E. C. Hirsch, T. Rooney, M. Ruberg, A. Brice, Parkin prevents mitochondrial swelling and cytochrome c release in mitochondria-dependent cell death. *Hum. Mol. Genet.* **12**, 517–526 (2003).
18. L. P. MacCormac, M. M. K. Muqit, D. J. Faulkes, N. W. Wood, D. S. Latchman, Reduction in endogenous *parkin* levels renders glial cells sensitive to both caspase-dependent and caspase-independent cell death. *Eur. J. Neurosci.* **20**, 2038–2048 (2004).
19. D. B. Wang, G. A. Garden, C. Kinoshita, C. Wyles, N. Babazadeh, B. Sopher, Y. Kinoshita, R. S. Morrison, Declines in Drp1 and parkin expression underlie DNA damage-induced changes in mitochondrial length and neuronal death. *J. Neurosci.* **33**, 1357–1365 (2013).
20. J. P. Anderson, D. E. Walker, J. M. Goldstein, R. de Laat, K. Banducci, R. J. Caccavello, R. Barbour, J. Huang, K. Kling, M. Lee, L. Diep, P. S. Keim, X. Shen, T. Chataway, M. G. Schlossmacher, P. Seubert, D. Schenk, S. Sinha, W. P. Gai, T. J. Chilcote, Phosphorylation of Ser-129 is the dominant pathological modification of α-synuclein in familial and sporadic Lewy body disease. *J. Biol. Chem.* **281**, 29739–29752 (2006).
21. H. Fujiwara, M. Hasegawa, N. Dohmae, A. Kawashima, E. Masliah, M. S. Goldberg, J. Shen, K. Takio, T. Iwatsubo, α-Synuclein is phosphorylated in synucleinopathy lesions. *Nat. Cell Biol.* **4**, 160–164 (2002).
22. K. K. K. Chung, Y. Zhang, K. L. Lim, Y. Tanaka, H. Huang, J. Gao, C. A. Ross, V. L. Dawson, T. M. Dawson, Parkin ubiquitinates the α-synuclein-interacting protein, synphilin-1: Implications for Lewy-body formation in Parkinson disease. *Nat. Med.* **7**, 1144–1150 (2001).
23. T. Murakami, M. Shoji, Y. Imai, H. Inoue, T. Kawarabayashi, E. Matsubara, Y. Harigaya, A. Sasaki, R. Takahashi, K. Abe, Pael-R is accumulated in Lewy bodies of Parkinson's disease. *Ann. Neurol.* **55**, 439–442 (2004).
24. A. B. Cholanians, A. V. Phan, E. J. Ditzel, T. D. Camenisch, S. S. Lau, T. J. Monks, From the cover: Arsenic induces accumulation of α-synuclein: Implications for synucleinopathies and neurodegeneration. *Toxicol. Sci.* **153**, 271–281 (2016).
25. V. Bagga, S. B. Dunnett, R. A. Fricker, The 6-OHDA mouse model of Parkinson's disease – terminal striatal lesions provide a superior measure of neuronal loss and replacement than median forebrain bundle lesions. *Behav. Brain Res.* **288**, 107–117 (2015).
26. R. K. W. Schwarting, J. P. Huston, The unilateral 6-hydroxydopamine lesion model in behavioral brain research. Analysis of functional deficits, recovery and treatments. *Prog. Neurobiol.* **50**, 275–331 (1996).
27. M. Oliveras-Salvá, A. Van der Perren, N. Casadei, S. Stroobants, S. Nuber, R. D'Hooge, C. Van den Haute, V. Baekelandt, rAAV2/7 vector-mediated overexpression of alpha-synuclein in mouse substantia nigra induces protein aggregation and progressive dose-dependent neurodegeneration. *Mol. Neurodegener.* **8**, 44 (2013).
28. J. A. Killian, T. K. M. Nyholm, Peptides in lipid bilayers: The power of simple models. *Curr. Opin. Struct. Biol.* **16**, 473–479 (2006).
29. R. C. Page, S. Kim, T. A. Cross, Transmembrane helix uniformity examined by spectral mapping of torsion angles. *Structure* **16**, 787–797 (2008).
30. C. Vives-Bauza, C. Zhou, Y. Huang, M. Cui, R. L. A. de Vries, J. Kim, J. May, M. A. Tocilescu, W. Liu, H. S. Ko, J. Magrané, D. J. Moore, V. L. Dawson, R. Grailhe, T. M. Dawson, C. Li, K. Tieu, S. Przedborski, PINK1-dependent recruitment of Parkin to mitochondria in mitophagy. *Proc. Natl. Acad. Sci. U.S.A.* **107**, 378–383 (2010).
31. M. Bian, J. Liu, X. Hong, M. Yu, Y. Huang, Z. Sheng, J. Fei, F. Huang, Overexpression of parkin ameliorates dopaminergic neurodegeneration induced by 1- methyl-4-phenyl-1,2,3,6-tetrahydropyridine in mice. *PLOS ONE* **7**, e39953 (2012).
32. F. P. Manfredsson, C. Burger, L. F. Sullivan, N. Muzyczka, A. S. Lewin, R. J. Mandel, rAAV-mediated nigral human parkin over-expression partially ameliorates motor deficits via enhanced dopamine neurotransmission in a rat model of Parkinson's disease. *Exp. Neurol.* **207**, 289–301 (2007).
33. Y. Imai, M. Soda, R. Takahashi, Parkin suppresses unfolded protein stress-induced cell death through its E3 ubiquitin-protein ligase activity. *J. Biol. Chem.* **275**, 35661–35664 (2000).
34. H. Jiang, Y. Ren, J. Zhao, J. Feng, Parkin protects human dopaminergic neuroblastoma cells against dopamine-induced apoptosis. *Hum. Mol. Genet.* **13**, 1745–1754 (2004).
35. J.-H. Shin, H. S. Ko, H. Kang, Y. Lee, Y.-I. Lee, O. Pletinkova, J. C. Troconso, V. L. Dawson, T. M. Dawson, PARIS (ZNF746) repression of PGC-1α contributes to neurodegeneration in Parkinson's disease. *Cell* **144**, 689–702 (2011).
36. Y. Lee, D. A. Stevens, S.-U. Kang, H. Jiang, Y.-I. Lee, H. S. Ko, L. A. Scarffe, G. E. Umanah, H. Kang, S. Ham, T.-I. Kam, K. Allen, S. Brahmachari, J. W. Kim, S. Neifert, S. P. Yun, F. C. Fiesel, W. Springer, V. L. Dawson, J.-H. Shin, T. M. Dawson, PINK1 primes parkin-mediated ubiquitination of PARIS in dopaminergic neuronal survival. *Cell Rep.* **18**, 918–932 (2017).
37. S. C. Kumer, K. E. Vrana, Intricate regulation of tyrosine hydroxylase activity and gene expression. *J. Neurochem.* **67**, 443–462 (1996).
38. S. B. Berman, T. G. Hastings, Dopamine oxidation alters mitochondrial respiration and induces permeability transition in brain mitochondria: Implications for Parkinson's disease. *J. Neurochem.* **73**, 1127–1137 (1999).
39. G. Cohen, R. Farooqui, N. Kesler, Parkinson disease: A new link between monoamine oxidase and mitochondrial electron flow. *Proc. Natl. Acad. Sci. U.S.A.* **94**, 4890–4894 (1997).
40. H.-J. Lee, S.-J. Lee, Characterization of cytoplasmic α-synuclein aggregates. Fibril formation is tightly linked to the inclusion-forming process in cells. *J. Biol. Chem.* **277**, 48976–48983 (2002).
41. A. Björklund, S. B. Dunnett, The amphetamine induced rotation test: A re-assessment of its use as a tool to monitor motor impairment and functional recovery in rodent models of Parkinson's disease. *J. Park. Dis.* **9**, 17–29 (2019).
42. R. Di Maio, P. J. Barrett, E. K. Hoffman, C. W. Barrett, A. Zharikov, A. Borah, X. Hu, J. McCoy, C. T. Chu, E. A. Burton, T. G. Hastings, J. T. Greenamyre, α-Synuclein binds to TOM20 and inhibits mitochondrial protein import in Parkinson's disease. *Sci. Transl. Med.* **8**, 342ra78 (2016).

Acknowledgments: We thank many young scientists who were involved in this study for their technical assistance. **Funding:** This work was supported by grant of (i) an Edmond J. Safra Core Program for PD Research (14241 to D.J.) of The Michael J. Fox Foundation for Parkinson's Research (USA) and (ii) Preclinical Test Support of New Drug Development (HI18C1986) of the Ministry of Health and Welfare (Korea). The funders had no role in the study design, data collection and analysis, decision to publish, or preparation of the manuscript. **Author contributions:** Conception and design: D.J. Development of methodology and performed the experiments: E.C., Y.C., Jiae Park, Jaehyung Park, W. N., Y.J., Joonno Lee, H.L., S.P., S.H., S.K., Jongseok Lee, D.M., J.J., S.K., P.H.L., and D.J. Acquisition of data: D.J. Analysis and interpretation of data: P.H.L., H.E.R., and D.J. Writing, review, and/or revision of the manuscripts: E.C., Y.C., M.J., H.E.R., and D.J. Administrative, technical, or material support: D.J. Study supervision: D.J. **Competing interests:** D.J. is the founding scientist of Cellivery Therapeutics Inc. D.J. and all others including an advisor, H.E.R., who is affiliated to Vanderbilt University as an emeritus professor are employees of Cellivery Therapeutics Inc. Hereby, all the authors disclose a financial interest in the company. Cellivery Therapeutics Inc. has filed patents for "Advanced macromolecule transduction domain (aMTD) sequences for improvement of cell-permeability, polynucleotides encoding the same, method to identify the unique features of aMTDs comprising the same, method to develop the aMTD sequences comprising the same" under the name of D.J., and "Improved cell-permeable (iCP) Parkin recombinant protein and use

there of" under the name of D.J. The relevant application numbers are PCT/KR2015/008544 and PCT/KR2016/008174, respectively. aMTD patent is currently registered in the US (15/503117), KR (10-2017-7005079), JP (2017-510405), CA (2957501), and AU (2015304194). There are no further patents, products in development, or marketed products to declare. iCP-Parkin patent is currently registered in US (15/879664), JP (2018-503759), EP (16830820.3) and AU (2016299468). **Data and materials availability:** All data needed to evaluate the conclusions in the paper are present in the paper and/or the Supplementary Materials. The data that support the findings of this study are available from the corresponding author upon reasonable request through a material transfer agreement.

Submitted 6 November 2019
Accepted 7 February 2020
Published 29 April 2020
10.1126/sciadv.aba1193

Citation: E. Chung, Y. Choi, J. Park, W. Nah, J. Park, Y. Jung, J. Lee, H. Lee, S. Park, S. Hwang, S. Kim, J. Lee, D. Min, J. Jo, S. Kang, M. Jung, P. H. Lee, H. E. Ruley, D. Jo, Intracellular delivery of Parkin rescues neurons from accumulation of damaged mitochondria and pathological α-synuclein. *Sci. Adv.* **6**, eaba1193 (2020).